TECHNISCHE UNIVERSITÄT WIEN

VIENNA UNIVERSITY OF TECHNOLOGY

DIPLOMA THESIS

Molecular dynamics simulations of anesthetics in phospholipid bilayers

performed at

Austrian Institute of Technology (Seibersdorf), AIT

supervised by

Dr. rer. nat. Thomas Stockner (AIT)

Ao. Univ. Prof. Dipl.-Ing. Dr. techn. Harald Markum

written by

Hansjörg Jerabek

Table of Contents

Abstract

Since almost all biologically relevant cell membranes are formed by phospholipid bilayers, the investigation of the influence of anesthetics on the physical and chemical properties of these bilayers is essential for actually understanding the mechanism of anesthesia. In our research, molecular dynamics simulations of fully hydrated POPC bilayers containing the anesthetic ketamine in concentrations between 0 and 8% were performed. A variety of analysis methods were applied to the simulation data to obtain detailed information about membrane parameters that may change due to the presence of anesthetics. We especially focused our attention on the anesthetic induced variation of the lateral pressure profile, whose modification can effect membrane proteins like ion channels by changing their conformational equilibrium. The results clearly show that the anesthetic most likely resides at a certain height in the bilayer. Especially at that position, the lateral pressure gets more and more reduced with increasing concentrations, leading to relative differences of more than 10% compared to the unanesthetized membrane. The corresponding changes of the first and second moments of the lateral pressure applied to a simple geometric model of an ion channel confirm that the conformational equilibrium of the channel is significantly shifted even at low ketamine concentrations.

1 Introduction

All living organisms in nature are formed by cells, no matter whether they consist of only one, like bacteria, or of several thousands of billions of cells, like we humans. The cells are surrounded by membranes which have the function to separate them from their environment. Furthermore, the membrane must allow the transport of different kinds of material from the inside to the outside or vice versa and the transmission respectively reception of signals. Therefore special molecules called proteins are embedded in the membrane to make these interactions possible. While some proteins are integral parts on one side of the membrane, others are forming transmembrane structures that have contact to the inside as well as to the outside of the cell. Special kinds of transmembrane structures are ion channels which are the membrane proteins we will turn our main attention to. These channels are essential for controlling the potential difference between the interior and the exterior of the cell because they provide a selective transport of ions through the membrane. This is especially important for the transmission of neuronal signals because the activity of a neuron, meaning whether it sends a signal or not, depends on its membrane potential. In this way a change of the permeability of ion channels can lead to a modification of a neuron's transmission behavior. Thus the specified modification can lead to the same effect that anesthetics have: they inhibit the transmission of neuronal signals and thereby lessen or take away sensation. Therefore, anesthesia can be seen as a kind of dysfunction of neurons.

Even though most scientists working on the topic of anesthesia agree that the change of the membrane properties is responsible for its effect, the question how the membrane is influenced in detail still lacks of a final answer and thereby leads to controversial discussions. In general, there are two major theories trying to explain how an anesthetic can influence biological membranes and the proteins within:

- Binding theory

  The anesthetic is expected to directly bind to a membrane protein which leads to a change of the protein's conformation and thereby to its function and behavior.

- Membrane theory

  According to this theory, the anesthetic does not have any direct contact to a membrane protein but is expected to diffuse into the membrane. This leads to a modification of the membrane's physical and chemical properties and thereby influences the embedded proteins.

The main reason why neither of the two theories could be abolished or totally confirmed can be found in the lack of experimental methods available for studying cell membranes. Therefore, in order to get a better insight which theory should be preferred, computer simulations provide a very useful method for investigating the behavior of biological membranes.

In this thesis we are trying to find support for the membrane theory and thus we expect the anesthetics to diffuse into the membrane. The effect one expects from the intrusion of the anesthetic is a change of the pressure inside the membrane which can modify the functionality of proteins that reside in it in a pure mechanical way. Since the permeability of an ion channel is sensitive to its depth-dependent cross-sectional area, the increase or decrease of pressure at certain positions in the membrane leads to a change of the amount of energy needed for the transition of the channel from one thermodynamic state to another. This means that the probability that this transition takes place changes. Due to this pressure induced shift of the thermodynamic conformational equilibrium, the behavior of the ion channel can be altered in a way that it permanently allows ions to enter or leave the cell or stops letting them pass. For simplicity, we expect the ion channel to only have two states, namely an opened and a closed one. Both, the possibility that the change of pressure due to the presence of an anesthetic is responsible for the specified modifications, and the fact that the membrane theory gives a good and simple explanation why anesthetics with very different structures have the same effects on cells, were basically the reasons why we started our research on that topic. The reason why the experimental determination, which would lead to a verification or falsification of the theory we represent, is so difficult, are the enormous pressure differences of more than 1000 bar that occur at distances of only a few nanometers. This difference can be compared to the one between the pressure at the surface of the earth and a few thousand meters beyond the sea. Until now there has not been any reliable method found for measuring these pressures accurately. Nevertheless, various experimental methods provide information about different kinds of membrane properties, like area per lipid, x-ray form factors, deuterium order parameters etc. These properties can also be derived using the data obtained from computer simulations. A comparison allows to find out how well the simulations reproduce the physical and chemical properties of “real” membranes.

1.1 Phospholipids

Almost all cell membranes are formed by phospholipids which consist of glycerol, two fatty acids and a phosphate containing polar headgroup. The phospholipid we used to construct our membrane for the simulation is called POPC. This name is an abbreviation for its full chemical name 1-**p**almitoyl-2-**o**leoyl **p**hosphatidyl**c**holine.

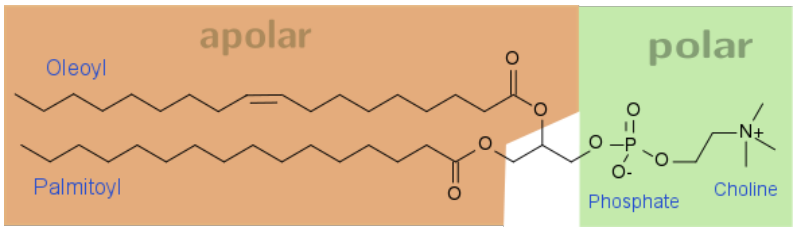

Fig. 1.1: Chemical components of POPC

Palmitoyl and oleoyl are fatty acids which are simple chains of carbon atoms with a carboxyl group at the end. The carboxyl group itself consists of a carbon atom, to which a double bonded oxygen and a hydroxy group (OH) are connected to. Because of the double bonded oxygen the fatty acids are also called acyl chains. If the carbons of the chain are just connected by single bonds, the fatty acid is called “saturated”. Otherwise, namely if double or triple bonds can be found, we talk about “unsaturated” chains.

While the palmitoyl chain consists of 16 carbon atoms and is saturated, the oleoyl fatty acid consists of 18 carbon atoms and has a double bond between the 9^{th} and the 10^{th} carbon, therefore it is an unsaturated acyl chain. The numbering of the carbons of the chain starts with the carboxyl carbon that carries the two oxygens.

Each of the two fatty acids is connected to a glycerol (propan-1,2,3-triol) molecule, a secondary alcohol. The connection is established by a condensation reaction. During this chemical reaction two molecules combine to a single one and emit a smaller molecule. In our case, the leaving molecule is water. The fatty acids and the glycerol are connected via their hydroxy groups, forming an ester bond.

A phosphate group is added to the third hydroxy group of the glycerol. This is again done by condensation. The phosphate group itself consists of a phosphorus with 4 connected oxygens, where one of the oxygens is negatively charged. This negative charge gets compensated by the positive charge of the nitrogen atom of the choline which is a primary alcohol and connected to the phosphate group. The phosphate and the choline group together are generally denoted as the headgroup of a phospholipid.

Due to the fact that one can use a big variety of different fatty acids and furthermore connect various molecular groups to the phosphate group, the number of different phospholipids, a cell membrane can be built with, is huge. Since each cell indeed uses a lot of diverse phospholipids, the surface is not uniform. This means that the membrane's local physical properties, and thus the effectiveness and functioning of the embedded proteins, strongly depend on the present phospholipid.

1.2 Bilayer membranes

Biological membranes are bilayers consisting of two phospholipid monolayers. The reason that the cell membrane does not consist of only monolayers can be found in the hydrophilicities of the different chemical groups of the phospholipids. While the headgroup is polar and thereby hydrophilic, the fatty acid chains are obviously hydrophobic. Monolayers are not stable in water because of the large energetic cost of the exposed hydrophilic-hydrophobic surface of the lipid-water interface. Thus two single layers form a bilayer, where the acyl chains point towards each other and the headgroups point towards the outside (water). In this way the hydrophobic core of the bilayer also hinders water molecules from diffusing through the membrane.

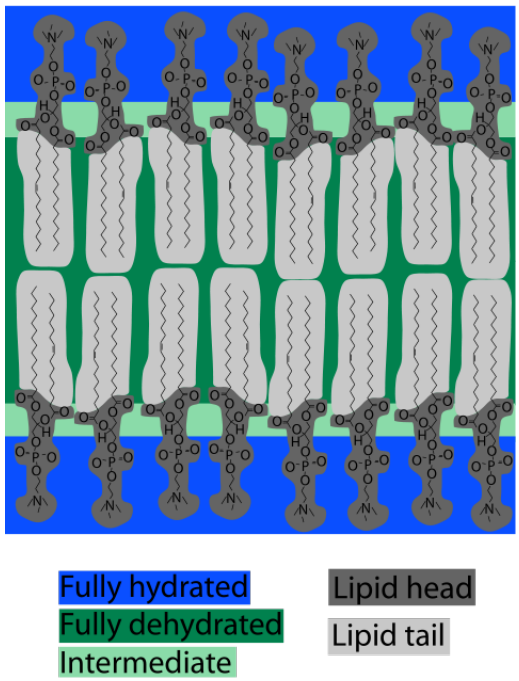

Fig. 1.2: Bilayer membrane

1.3 Membrane proteins

In general, proteins are biological catalysts and thus have the function to decrease the energy which is needed for executing a certain process, like a chemical reaction. For that reason proteins are essential for living cells and can be found in all kinds of organisms. Also the correct functioning of cell membranes strongly depends on specific proteins embedded in the membrane, so-called membrane proteins, which fulfill different purposes:

- Structural proteins

These proteins are connected to microfilaments in the cytoskeleton and thereby ensure the cell membrane's stability.

- Cell recognition proteins

  They allow cells to identify each other which is especially important for the interactions between them, for example during an immune response.

- Receptor proteins

  They serve as connection between the cell's interior and exterior because they transmit signals when a certain molecule binds to them. In this way the signal can be forwarded without the molecule entering the cell.

- Transport proteins

  These proteins either passively or actively (using ATP) enable the transport of molecules and ions into or out of the cell. As already mentioned, especially the ion channels are very important for neurons because they make the adjustment of their membrane potential possible.

Furthermore, membrane proteins can be divided into two subclasses depending on their position relative to the membrane:

- Integral membrane proteins

  Transmembrane proteins span the total membrane, are permanently attached to the membrane and need an apolar solvent to be displaced.

- Peripheral membrane proteins

  These proteins are only temporarily attached to the membrane or to integral membrane proteins.

1.4 Protein conformations

All known physical systems try to reach a global or at least local energy minimum; the same behavior holds for proteins. A structure of the protein occupying such a minimum is thereby at least temporarily stable and denoted as a conformation or state of the protein.

The conformation can change when the forces acting on a protein are modified. This means that the conformation always depends on the protein's environment. In our case, we expect this environment to be changed by the

presence of an anesthetic.

1.5 Anesthetics

Substances that cause anesthesia are called anesthetics. They have the purpose to temporarily block or take away the sensation and thus allow patients to undergo surgery and other procedures which would otherwise be very painful. In general, the effect of anesthesia can include:

- Analgesia - blocks the sensation of pain
- Hypnosis - leads to unconsciousness
- Amnesia - prevents memory formation
- Paralysis - leads to an inhibition of movement and muscle tone

Because of all these effect, anesthetics are widely used in human and veterinary medicine. The general use of anesthetics for surgeries started in the 19th century. Even though the first public demonstration of an anesthetic-aided surgery (using diethyl ether) took place in 1846, the question how anesthetics effect cells in detail, is still unanswered after more than 160 years. The influence on human bodies for most of the anesthetics used nowadays is quite well known, due to the many empirical data available. However, although we know the effects of anesthetics on organisms, we are not sure about their mode of functioning. Due to these circumstances, a creation of new anesthetics is not easily possible.

All the uncertainties concerning the topic of anesthesia result in a lot of side effects that can occur, even today. Besides the risk of suffering from different kinds of brain damage, it is possible that one of the general anesthetic effects, like amnesia or paralysis, does not vanish after an operation and thereby harms the patient. The main problem one has to keep in mind is that the therapeutic window of anesthetics is only very small. This means that there is only little difference between a dose leading to a recognizable effect, and a dose which is toxic. In combination with the fact, that the constitution of patients can strongly vary, which has to lead to an adaption of the dose, one has to mention that being anesthetized even nowadays bears a risk.

The anesthetic we turn our attention to is ketamine, also known as 2-(2-chlorophenyl)-2-methylamino-cyclohexane-1-one. It has been developed by Parke-Davis in 1962 and is widely used in human and veterinary medicine. Ketamine is pharmacologically classified as an NMDA receptor antagonist meaning that it inhibits the action of **N**-**m**ethyl **d**-**a**spartate receptor. In general NMDA receptor antagonists are known to induce a state called dissociative anesthesia which is marked by amnesia, analgesia and catalepsy. Besides those of general anesthesia, ketamine has several

additional effects:

- Hallucinations
- Bronchodilation
- Increase of heart rate
- Elevation of blood pressure

Since ketamine has first been given to soldiers in the Vietnam war, they were the first ones who reported experiencing hallucinations under the influence of this anesthetic drug. For that reason, it is usually not used as a primary drug, but often applied in combination with a sedative drug, like for example benzodiazepine. Because of this negative side effect, ketamine would probably not be used today, if it would not have its advantages. Due to the bronchodilation and the increase of the heart rate as well as the blood pressure, it is used for emergency surgery. These positive effects on the circulatory and respiratory system can allow to perform surgeries without the use of additional special equipment, like for ventilation.

Chemically, ketamine consists of two ring structures (see Fig. 1.3), namely a phenyl- and a cyclohexane-ring. A chlorine atom is connected to the phenyl and an oxygen atom and a methylamino group are connected to the cyclohexane. As most anesthetics, ketamine is mainly hydrophobic, but also has polar and thereby hydrophilic parts, like the oxygen atom. The hydrophobicity is another reason why we expect the anesthetic to diffuse into the membrane, since it would take a lot of additional surface energy for the anesthetic, if it would reside in a polar medium, like water.

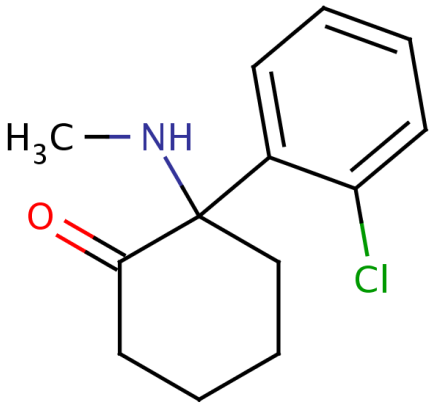

Fig. 1.3: Structure of ketamine

The overview of the remainder of this thesis is as follows. In Chapters 2 and 3 we provide the theoretical basics of the computer simulations and the analysis methods. In Chapter 4 the settings of the performed simulations are described and the obtained results are presented and discussed in Chapter 5. In the last chapter we will then draw conclusion from all results and give an outlook to future research.

2 Theory of molecular dynamics simulations

In general, molecular dynamics (MD) simulations allow to estimate the temporal evolution of a system in atomic detail. This is done by solving Newton's equations of motion for all atoms of a given system:

$$\vec{F}_i = m_i \frac{\partial^2 \vec{r}_i}{\partial t^2} \quad . \tag{2.1}$$

The forces can be obtained from the gradient of the potential V:

$$\vec{F}_i = -\frac{\partial V(\vec{r}_i)}{\partial \vec{r}_i} = -\vec{\nabla}_i V(\vec{r}_i) \quad . \tag{2.2}$$

During every time step of the simulation all equations have to be solved and different kinds of boundary conditions, like constance of temperature or pressure, have to be fulfilled. In this chapter all these theoretical basics of MD simulations will be presented and discussed [1].

2.1 Force field

Depending on the system of interest, different kinds of interactions between atoms and molecules can occur. Various force fields have been developed for describing these interactions. Due to the several simplifications that have to be made when determining the total energy, there is no force field which describes all systems well, but certain force fields are optimized for certain purposes. This can be done by simulating representative systems and comparing simulated parameter values with those obtained from experiments. If the consistency is not satisfying, various force field parameters can be fitted until the best agreement is found.

Most of the commonly used force fields have a similar form and include Coulomb and Lennard-Jones terms, harmonic bond stretching, angle bending and a torsional energy function. While Coulomb and Lennard-Jones interactions are denoted as “nonbonded” interactions, terms like for the harmonic bond stretching and angle bending, are called “bonded”. Of course, Coulomb and Lennard-Jones potentials are also responsible for bonding, but to calculate for example the binding energy for two atoms of a molecule, one would have to take the overlap of their atomic orbitals and other quantum mechanical circumstances into account. This would take a lot

of time during a simulation run. For that reason the binding energies are approximated by harmonic oscillator potentials, using empirical information like the average distance between the two bonding atoms or the angle of the triangle spanned by three atoms etc. On the one hand this allows to simplify the simulations, but on the other hand one always has to keep in mind that the accuracy of a simulation primarily depends on the accuracy of the empirical values that have been used to optimize the force field.

We used the Berger lipids [2] for describing the POPC lipids, OPLS-AA force field [3] for the ketamine drug and we applied the SPC water model [4]. OPLS-AA stands for **O**ptimized **P**otentials for **L**iquid **S**ystem – **A**ll-**A**tom. It has been optimized for liquid systems and works well together with the Berger lipids [5]; it can therefore be used for simulating hydrated lipid bilayers. The suffix “All-Atom” means that all atoms, including the hydrogens, are sites for nonbonded interactions. In contrast to this, in United-Atom (UA) force fields these sites are only placed on all non-hydrogen atoms and on hydrogens attached to heteroatoms or carbons in atomic rings. So while for example propanol (C_3H_7OH) has 5 interaction sites in UA, it has 12 in AA representations. Even though UA force fields are computationally attractive, AA force fields allow more flexibility for charge distributions and torsional energies and thereby are in better agreement with experimental result. The Berger lipids are a very well tested UA force field with the nonbonded parameters based on OPLS-UA. The advantage of this representation is a speed gain of one order of magnitude. This is essential, as membrane properties are very slow to equilibrate.

In the OPLS-AA force field the nonbonded interaction energy between two molecules x and y is represented by

$$\begin{aligned} E_{xy} &= E_{xy,\,COULOMB} + E_{xy,\,LENNARD-JONES} \\ &= \sum_{i\in x}\sum_{j\in y}\frac{q_i q_j e^2}{r_{ij}} f_{ij} + 4\sum_{i\in x}\sum_{j\in y}\epsilon_{ij}\left[\left(\frac{\sigma_{ij}}{r_{ij}}\right)^{12} - \left(\frac{\sigma_{ij}}{r_{ij}}\right)^{6}\right] f_{ij} \end{aligned} \quad , \tag{2.3}$$

where q_i*e is the charge of the i^{th} atom, r_{ij} is the distance between the i^{th} and the j^{th} atom and f_{ij} is a scaling factor which is 1, except for intramolecular 1,4 interactions. The Lennard-Jones (Van der Waals) parameters σ_{ij} and ε_{ij} can be obtained using the following standard combining rules:

$$\begin{aligned} \sigma_{ij} &= \sqrt{\sigma_{ii}\sigma_{jj}} \\ \epsilon_{ij} &= \sqrt{\epsilon_{ii}\epsilon_{jj}} \end{aligned} \quad . \tag{2.4}$$

For the bonded interaction terms, the harmonic oscillator potentials for the bond stretching and the angle bending are given by

$$E_{bond} = \sum_{i \in bonds} k_{r,i}(r_i - r_{i,0})^2 \tag{2.5}$$

and

$$E_{angle} = \sum_{i \in angles} k_{\theta,i}(\theta_i - \theta_{i,0})^2 \quad , \tag{2.6}$$

with k_r and k_θ being scaling constants and r_0 and θ_0 being empirical values for bond lengths and bond angles.

Additionally, one has to take the intramolecular torsional energy

$$\begin{aligned} E_{torsion} = \frac{1}{2}\sum_i & V_1^i[1+\cos(\phi_i + f_1^i)] + V_2^i[1+\cos(2\phi_i + f_2^i)] \\ & + V_3^i[1+\cos(3\phi_i + f_3^i)] + V_4^i[1+\cos(4\phi_i + f_4^i)] \end{aligned} \tag{2.7}$$

into account, where Φ denotes the dihedral angle, V_j are the coefficients in the Fourier series and f_j are phase angles.

2.2 Algorithms

2.2.1 Temporal evolution

To determine how our phospholipid bilayer evolves in time, the leap-frog algorithm is used for solving the equations of motion for each atom [6]:

$$\begin{aligned} \vec{v}(t + \frac{\Delta t}{2}) &= \vec{v}(t - \frac{\Delta t}{2}) + \frac{\vec{F}(t)}{m}\Delta t \\ \vec{r}(t + \Delta t) &= \vec{r}(t) + \vec{v}(t + \frac{\Delta t}{2})\Delta t \end{aligned} \quad , \tag{2.8}$$

with Δt being the time step of the simulation. By knowing a particle's position and the forces acting on it at the time t and by knowing its velocity at time t – Δt/2, one can calculate the position of this particle at the time t + Δt. This algorithm can be written as

$$\vec{r}(t + \Delta t) = 2\vec{r}(t) - \vec{r}(t - \Delta t) + \frac{\vec{F}(t)}{m}\Delta t^2 + O(\Delta t^4) \quad , \tag{2.9}$$

which is called the Verlet algorithm [7]. By repeating this calculations after every time step and updating all particles' positions, one can obtain the trajectory of each atom and thereby of the whole system. There are of course better algorithms available for computing the temporal evolution, like the Runge-Kutta [8] or the Adams-Bashforth [9] algorithm, but the one used here is very simple, robust and computationally attractive.

For starting a simulation at t = 0 we need an initial structure to start with. Since the leap-frog algorithm is used, we do on the one hand need the position of all atoms at t = 0, and on the other hand the velocities at t = -Δt/2. Due to the fact that in most cases only the structure itself, meaning the position of each atom, is known, the velocities have to be randomly generated. Therefore, the atoms' velocity distribution is expected to be Maxwellian:

$$p(v_i) = \sqrt{\frac{m_i}{2\pi k_b T}} \exp\left(\frac{-m_i v_i^2}{2 k_b T}\right) \quad . \tag{2.10}$$

Here m_i and v_i denote the mass and the velocity of the i^{th} atom, k_b is Boltzmann's constant and T is the temperature of the system.

Due to the randomly generated particle starting-velocities and in most cases randomly placed molecular structures, the system is not at equilibrium at the beginning of a simulation. In general, the system is said to be in thermodynamic equilibrium when it shows only thermal fluctuations around a mean value, while remaining in the same conformational basin. As long as the system is not disturbed, like for example through the occurrence of an external force, it is stable. Obviously it would not make sense to derive representative membrane parameters if this state is not reached. For all the performed analyses we therefore only used simulation data of the equilibrated system.

2.2.2 Periodic boundary conditions

Periodic boundary conditions are used to minimize edge effects caused by the finite system size. It is called periodic boundary because for the calculations the system is spatially surrounded by identical images of itself. This can be done by copying the system and translating it by a certain vector (Fig. 2.1). Thereby the computational artifact caused by unwanted boundaries like vacuum is replaced by the artifact of periodic conditions. When simulating crystals such conditions are desired, but for non-periodic systems the generated periodicity itself causes errors. Since these errors are much smaller than the ones which would arise from unwanted boundaries, periodic boundary conditions are also applied for simulations of liquids and solutions.

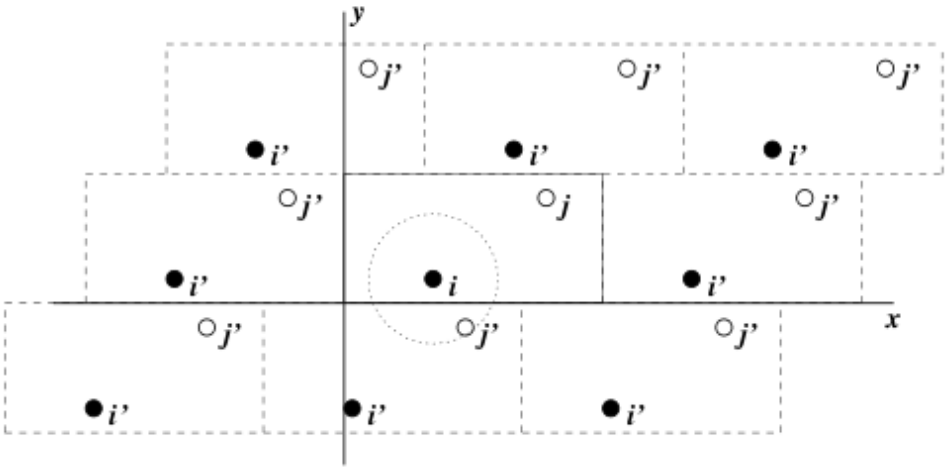

Fig. 2.1: Periodic boundary condition and minimum image convention [1]

The use of periodic boundary conditions leads to the implementation of the so-called minimum image convention (Fig. 2.1): For nonbonded interactions only one, namely the nearest, image of each particle is considered for the calculations. Otherwise further side effects would occur due to interaction between identical images of particles.

2.2.3 Cutoff radii

In the simulation every atom is expected to only interact with particles that are within the cutoff radius. This restriction reduces the computational effort for evaluating the nonbonded energy terms. Due to the minimum image convention and because one does not want an atom to interact with a copy of itself, the cutoff radius must be smaller than half the shortest box vector:

$$R_{cutoff} < \frac{1}{2} min(\|\vec{a}\|, \|\vec{b}\|, \|\vec{c}\|) \quad . \tag{2.11}$$

Here, **a**, **b** and **c** are the vectors that span the simulation box and are called box vectors.

2.2.4 Center-of-mass motion removal

Since the system's center-of-mass motion would lead to an unwanted translation, the corresponding velocity is subtracted from each particle after every time step [10]. Thereby the center-of-mass velocity is almost zero as long as no external forces act on the system. This procedure has to be executed after every time step to prevent center-of-mass motions caused by numerical uncertainties.

2.2.5 Constraints

Several constraints have to be fulfilled to keep for example the bond length constant. Therefore, it is necessary to implement algorithms that keep atoms at constant distances, since the velocities between bonded atoms do in most cases not point into the same direction. Thus, from one time step in the simulation to the next, the particles may drift apart. Due to this so-called “unconstrained” update the need arises to reestablish the bond lengths according to the force field settings.

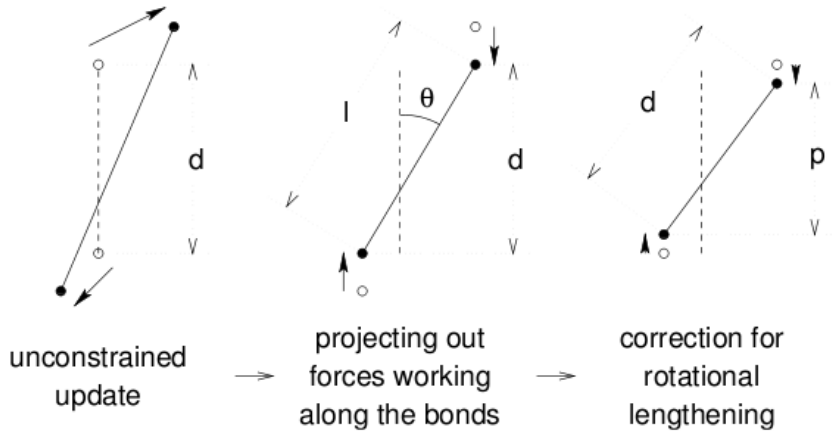

Fig. 2.2: Constraints [1]

For our simulation two different algorithms, namely the Shake [11] and the Lincs [12] algorithm were used. While the Lincs algorithm is faster and more stable than Shake, it can only be used for bond and angle constraints. As an example, Fig. 2.2 shows how the Lincs method works: At first, the projections of the new bonds that exceed the old bonds are set to zero and afterwards the correction for the lengths of the bonds is applied.

2.2.6 Kinetic energy and temperature

The total kinetic energy of a system is given by

$$E_{kin} = \sum_{i=1}^{N} \frac{m_i v_i^2}{2} \quad , \tag{2.12}$$

with N being the number of particles the system consists of. Since the equipartition theorem says that in thermal equilibrium the energy is shared equally among all degrees of freedom, the system's temperature can be calculated using the relation

$$E_{kin} = n_f \frac{k_b T}{2} \quad , \tag{2.13}$$

where n_f is the total number of degrees of freedom. For our system this number is given by

$$n_f = 3N - n_c - n_{comm} \quad . \tag{2.14}$$

Here n_{comm} = 3 denotes the degrees of freedom of the center-of-mass motion, and n_c is the number of constraints imposed on the system.

Due to numerical uncertainties and different kinds of particle drifts that can occur in the simulation, it is necessary to control the temperature of the system. This is done by temperature coupling algorithms. In the frequently used Berendsen algorithm [13] the deviation of the system's temperature T from the temperature T_0 of the heat bath, it is expected to be connected with, is assumed to behave according to the following relation

$$\frac{dT}{dt} = \frac{T_0 - T}{\tau} \quad . \tag{2.15}$$

This means that the deviation decays exponentially with a time constant τ. To suppress fluctuations of the kinetic energy the Berendsen thermostat is used to scale the velocities by a factor

$$\lambda = \sqrt{1 + \frac{\Delta t}{\tau_T}\left[\frac{T_0}{T(t - \Delta t/2)} - 1\right]} \quad . \tag{2.16}$$

The constant τ_T is close to, but not exactly the same as τ. Due to this simple velocity rescaling, the generated ensemble is not canonical. Therefore we used the so-called velocity rescaling thermostat for our simulations [14]. It consists of the Berendsen thermostat with an additional stochastic term for the kinetic energy:

$$dE_{kin} = (E_{kin,0} - E_{kin})\frac{\Delta t}{\tau_T} + 2\,dW\sqrt{\frac{E_{kin}E_{kin,0}}{\tau_T n_f}} \quad . \tag{2.17}$$

Thus the system's kinetic energy distribution is the same as of a canonical ensemble. In Eq. 2.17 $E_{kin,0}$ is the kinetic energy at T = T_0 and dW is a Wiener process.

2.2.7 Pressure and virial tensor

The pressure tensor can be computed from

$$\boldsymbol{P} = \frac{2}{V}(\boldsymbol{E}_{kin} - \boldsymbol{\Xi}) \quad , \tag{2.18}$$

where V is the volume of the simulation box and **Ξ** is the so-called virial tensor:

$$\boldsymbol{\Xi} = -\frac{1}{2}\sum_{i<j} \vec{r}_{ij} \otimes \vec{F}_{ij} \quad . \tag{2.19}$$

F_{ij} and r_{ij} are the force respectively the distance between the i^{th} and the j^{th} atom. In case of an isotropic system the scalar pressure is given by

$$P = \frac{trace(\boldsymbol{P})}{3} \quad . \tag{2.20}$$

Like for the temperature, also pressure coupling algorithms are used to maintain constant pressure. Applying again the Berendsen algorithm [13] for coupling, we assume that

$$\frac{d\boldsymbol{P}}{dt} = \frac{\boldsymbol{P}_0 - \boldsymbol{P}}{\tau_P} \quad , \tag{2.21}$$

in analogy to Eq. 2.15. Since the pressure is given by a tensor, a matrix has to be used for rescaling, namely

$$\boldsymbol{\mu}(t) = \boldsymbol{\delta} - \frac{\Delta t}{3\tau_P}\boldsymbol{\beta}\left(\boldsymbol{P_0} - \boldsymbol{P}(t)\right) \quad , \tag{2.22}$$

with **δ** being the Kronecker delta and **β** denoting the isothermal compressibility of the system. While for temperature coupling the velocities are modified, the coordinates and box vectors have to be rescaled for pressure coupling.

2.2.8 Neighbor searching

Neighbor or pair lists are used because it takes a high computational effort to identify the particles a certain atom interacts with (nonbonded interaction). Regarding the minimum image convention and cutoff restrictions, these lists are generated for all particle pairs, typically every 20 fs. Instead of recalculating them during the next step, one expects that the covered

distance of each particle is so small that the pairs do not change and thereby the previously generated list does not have to be updated.

2.2.9 Energy minimization

Energy minimization simulations have to be done before starting a simulation. This is necessary because in most cases the system is artificially created using algorithms which randomly place and rotate certain molecules in the simulation box. Due to the random positioning the energy of the initial system is not minimal which would lead to large forces acting on the atoms at the beginning of the simulation. Thereby some atoms could be accelerated so much that they cover a distance of several times the simulation box length during a single time step. In this way they would end up far away from the position they ought to be and that would distort the simulation's result.

In general, there are three frequently used algorithms available for performing energy minimization simulations: The steepest descent, the conjugate gradient and the Limited-memory Broyden-Fletcher-Goldfarb-Shanno quasi-Newtonian minimizer (L-BFGS) algorithm [15]. In most cases the steepest descent is used because it is easy to implement, robust and efficient enough, while the other two fail to find a decent minimum if the starting coordinates are bad. At first the potential energy and the forces are computed. The new position of all particles in the next step is then given by

$$\boldsymbol{r}_{n+1} = \boldsymbol{r}_n + \frac{\boldsymbol{F}_n}{max_i(|F_{i,n}|)} h_n \quad , \tag{2.23}$$

where **r** and **F** are the 3N-dimensional positions and forces for all atoms and h is the maximum displacement. The indices n and n+1 refer to the n^{th} and $(n+1)^{th}$ step. If the potential energy of the system at the next step is smaller than before, the new coordinates are accepted and h_{n+1} is set to 1.2 h_n. If this is not the case, the coordinates are rejected and h_n = 0.2 h_n. The algorithm stops either when the maximum of the absolute values of the force components is smaller than a specified value, or after a specified number of force evaluations.

Since the steepest descent method simply takes a step into the direction of the negative gradient, its convergence can be slow, especially close to the local minimum. In contrast to this, the conjugate gradient algorithm converges faster because it uses gradient information from previous steps. The L-BFGS method, which can also be used, is comparable to the conjugate gradient and converges faster in certain cases.

2.3 Limitations

Due to the fact that various approximations concerning the calculations have to be implemented in order to make MD simulations computationally attractive, one always has to keep the limitations in mind:

- The simulations are classical

  The use of Newton's equations of motion automatically implies that classical mechanics is used to describe the motion of atoms. For most particles at normal temperatures this is sufficient, but there are exceptions: The motion of protons is typically of quantum mechanical character because a proton may tunnel through a potential barrier in the course of a transfer over a hydrogen bond. Such processes cannot be properly treated by classical dynamics. Furthermore the statistical mechanics of a classical harmonic oscillator differs appreciably from that of a real quantum oscillator when the resonance frequency approximates or exceeds k_bT/h.

- Force fields are approximate

  The force fields provide the total energy and the forces acting on a system's atoms. Thus the accuracy of the simulation is determined by the accuracy of the empirically obtained force field parameters. Furthermore, only pairwise two body interactions are taken into account.

- Boundary conditions are unnatural

  Internal correlations between the periodic images can bias the results, especially when simulating small systems. The wavelength of membrane undulations for example can not be larger than the length of the simulation box. For the systems we studied (box dimensions ~10 nm) the effects of the boundary conditions can be neglected.

- Long-range interactions are cut off

  Nonbonded interactions have to be cut off after some distance because of computational efficiency. Van der Waals interactions are neglected beyond the cutoff. Electrostatic interactions are typically treated by a PME model [16] beyond the cutoff.

- Conservative force fields are used

  In MD simulations the electrons are assumed to instantaneously adjust their dynamics when the positions of the atoms change. This is known as Born-Oppenheimer

approximation and leads to the fact that the force field is only dependent of the position of the atoms and not of the position of the electrons (conservative force field). Furthermore the electrons are assumed to remain in their ground state. Due to this, excited states, electron transfer processes and chemical reactions can not be described.

- Limited sampling

  The position of all particles in the simulation is not saved after every time step because the stored information would use too much space on the hard disk drive. Thus an output is only performed once in a few hundred time steps. This limited sampling and the corresponding lack of information affect the statistical averages that have to be calculated in various analysis methods.

3 Theory of analysis methods

3.1 Area per lipid

The area per lipid is a measure for the lateral size of a lipid molecule:

$$A_L = \frac{2 L_x L_y}{N_L} \quad , \tag{3.1}$$

with L_x and L_y being the size of the system in x- and y-direction and N_L being the number of lipids the bilayer consists of. An increase of the area per lipid corresponds to a lateral expansion of the system, but thereby leads to a decrease of height because its volume remains approximately constant. This is the case because the “creation” of additional volume is energetically disadvantageous.

3.2 Position distribution function

The position distribution function $f_{position}$ is proportional to the probability to find a molecule or atom at a certain vertical position z inside the membrane. Since the position of a molecule or atom can be derived from the location of its electrons, the position distribution can be obtained by normalizing the electron density distribution:

$$\int_{-h}^{h} \rho_{electron}(z)\, dz = \epsilon \rightarrow \int_{-h}^{h} \frac{\rho_{electron}(z)}{\epsilon} dz = 1$$
$$f_{position} = \frac{\rho_{electron}(z)}{\epsilon} \quad . \tag{3.2}$$

The constant h in the limits of the integrals denotes the half size of the simulation system in the z-direction, meaning that 2h is the total height.

3.3 Angle distribution function

The angle distribution function is proportional to the probability to measure a certain angle α between the vector connecting two molecular groups and the vector pointing towards the bilayer normal:

$$\alpha(\vec{x}_1, \vec{x}_2) = \arccos\left(\frac{(\vec{x}_2 - \vec{x}_1) * \vec{e}_z}{|\vec{x}_2 - \vec{x}_1|}\right) \quad . \tag{3.3}$$

The vectors $\mathbf{x}_n$ are the coordinates of the center of the n^{th} atom or molecule, respectively, and $\mathbf{e}_z$ is the unit vector along the z-axis. Like before, the integral over the angle distribution function itself is normalized to 1.

3.4 Deuterium order parameter

The deuterium order parameter S_{CD}, which in remainder of this thesis will also simply be denoted as order parameter, is a measure for the alignment of the carbon atoms of an acyl chain compared to the bilayer normal z. This parameter can be measured experimentally using nuclear magnetic resonance (NMR) and complementarily it can be computed from the simulation data. The comparison indicates how well the simulation reproduces the bilayer. The prefix “deuterium” arises from the fact that for NMR experiments the hydrogen (1 proton, 1 electron) is replaced by deuterium (1 proton, 1 neutron, 1 electron).

For obtaining the order parameter one has to introduce the order parameter tensor

$$S_{ij} = \frac{1}{2}\langle 3\cos\theta_i \cos\theta_j - \delta_{ij} \rangle \quad , \tag{3.4}$$

where Θ_i is the angle between the i^{th} molecular axis (i,j=x,y,z) and the bilayer normal and δ_{ij} is the Kronecker delta. The average in Eq. 3.4 runs over all lipids in the membrane and over all time frames used for the analyses. Usually the molecular axes for the methylene groups of saturated acyl chains are defined as follows [17]: The x-axis is parallel to the vector connecting the two hydrogen atoms and the y-axis bisects the angle spanned by the two vectors from the carbon atom to the hydrogens. The z-axis is the normal to the plane spanned by the x- and y-axis (see Fig. 3.1).

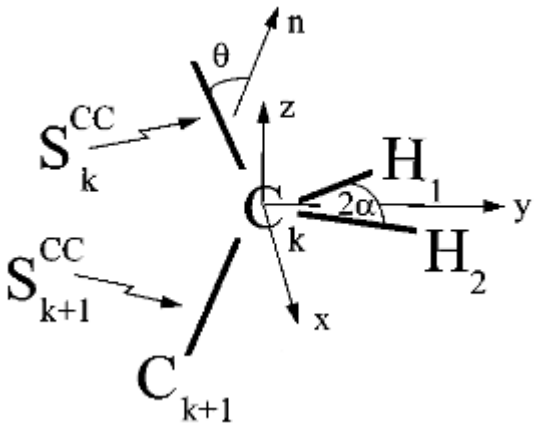

Fig. 3.1: Molecular axes of methylene group [17]

Using this coordinate system, the two deuterium order parameters for a saturated acyl chain carbon are given by

$$S_{CD1}^{SAT} = \frac{2S_{xx}}{3} + \frac{S_{yy}}{3} - \frac{2\sqrt{2}S_{xy}}{3}$$
$$S_{CD2}^{SAT} = \frac{2S_{xx}}{3} + \frac{S_{yy}}{3} + \frac{2\sqrt{2}S_{xy}}{3} \quad . \tag{3.5}$$

Assuming that the deuterium atoms are identical, S_{xy} must be zero and the order parameter can then be calculated using

$$S_{CD}^{SAT} = \frac{2S_{xx}}{3} + \frac{S_{yy}}{3} \quad . \tag{3.6}$$

Applying a similar geometric model for unsaturated acyl chains, it can be shown [17] that the order parameter for unsaturated carbons is given by

$$S_{CD}^{UNSAT} = \frac{S_{zz}}{4} + \frac{3S_{yy}}{4} \mp \frac{\sqrt{3}S_{yz}}{2} \quad , \tag{3.7}$$

where the last term has to be added or subtracted depending on which carbon of the double bond is concerned.

For the analyses the position of the hydrogen atoms need not directly be available as the coordinates of the protons can be constructed from the position of the carbon atoms. Due to the tetrahedral geometry of the methylene groups, the angle between the vectors from the carbon to the hydrogens is the same as between the vectors from the carbon to the next

and previous one. Using the same axes model as for the saturated case, a recursion relation, which allows to calculate the carbon-deuterium from the carbon-carbon order parameters, can be derived:

$$-2S_{CD}^{k} = S_{CC}^{k} + S_{CC}^{k+1} \quad . \tag{3.8}$$

In this case S^{k}_{CC} is the carbon-carbon order parameter of the k^{th} carbon atom.

Looking at

$$S_{zz} = \frac{1}{2}\langle 3\cos^2\theta_z - 1\rangle \tag{3.9}$$

as an example, one can figure out which values the components of the order parameter tensor can take: They range from 1 to -1/2, where -1/2 means that the chain is completely ordered along the z-axis and 1 that it is fully ordered perpendicular to the z-axis. Since the order along the z-axis is maximal for -1/2 and minimal for 1, $-S_{CD}$ is shown in all this thesis' figures to relate a positive change of the order parameter to an increase of order.

3.5 X-ray form factor

The form factor F(q) is a measure for the x-ray scattering amplitude, meaning that it contains the information how x-rays are scattered by the electron clouds of the atoms when passing a bilayer. Since x-ray scattering is a common method to study membrane structures, a lot of experimental data is available for the comparison with the results obtained from simulations.

The form factor is obtained by Fourier-transforming the difference between the electron density of the system and the electron density of bulk water [18]:

$$\begin{aligned} F(q) &= \int_{-h}^{h} (\rho_{e,system}(z) - \rho_{e,bulk\,water})\cos(qz)\,dz \\ &= \int_{-h}^{h} \rho_{e,system}(z)\cos(qz)\,dz - \frac{2\,\rho_{e,bulk\,water}\sin(qh)}{q} \end{aligned} \quad . \tag{3.10}$$

3.6 Mean square displacement and diffusion coefficients

The diffusion coefficient D allows to estimate the distance a randomly walking particle (Brownian motion) covers over a certain time and is at long

time scales proportional to the mean square displacement $d^2(t)$:

$$d^2(\tau)=\frac{1}{T-\tau}\int_{t=\tau}^{T}\left|\vec{r}(t)-\vec{r}(t-\tau)\right|^2 dt$$

$$d^2(n\cdot\Delta t)=\frac{1}{N-n+1}\sum_{i=n}^{N}\left|\vec{r}(i\cdot\Delta t)-\vec{r}((i-n)\cdot\Delta t)\right|^2 \quad . \tag{3.11}$$

In Eq. 3.11, T is the total simulation time, Δt is the time step and N is the number of time steps needed for the total simulation.

With

$$\lim_{t\to\infty} d^2(t)=2\cdot d_f\cdot D\cdot t \quad , \tag{3.12}$$

where d_f is the number of the particle's degrees of freedom, the diffusion coefficient can be derived from the slope of the mean square displacement.

3.7 Pressure profile

The pressure profile shows the depth-dependence of the pressure inside the membrane. One could claim that since the pressure is proportional to a force, a pressure different from zero could lead to a movement of certain parts of the membrane and would thereby destabilize it. But as long as the total pressure, which is in this case the integral over the pressure along the bilayer normal, is zero, the membrane is stable. Besides for the mechanical stability this is also a criterion that the membrane has reached its equilibrium state.

The reason why the pressure varies along the bilayer normal can be found in the different kinds of interactions that occur inside the membrane. Three main interaction regimes are located at different depths:

- Headgroup

  The headgroups of the phospholipids tend to mutually repulse each other. Therefore a positive pressure can be found at the height where the headgroup is most likely to reside.

- Lipid-water interface

  The lipid-water interface can be found close to the membrane-water interface, but it is located a bit closer to the bilayer center because the water molecules can slightly enter the membrane. In this region a large lateral tension (=negative pressure)

occurs. This tension arises from the cost of free energy caused by the contact of the water molecules with the hydrophobic carbon chains of the phospholipids and leads to an attraction of the acyl chains at that height. The attraction has the effect that it prevents the water molecules from entering the hydrophobic core.

- Center

  In the center of the bilayer the mutual repulsion of the carbon chains is the dominant interaction and leads to a positive pressure. In this case the interaction is steric and entropic: The carbon chains tend to increase the distance to each other because thereby they can increase their entropy. In this way one could also describe this interaction as a transition to a less ordered state of the chains.

For the calculation of the pressure profile the Irving-Kirkwood contour is used [19]. The bilayer is subdivided into lateral slices with a thickness of 0.1 nm for which the local pressure tensor

$$\boldsymbol{p}_{slice}(z) = \frac{1}{\Delta V}\left[\sum_{i \in slice} m_i \boldsymbol{v}_i * \boldsymbol{v}_i - \sum_{i<j} \boldsymbol{F}_{ij} * \boldsymbol{r}_{ij} f(z, z_i, z_j)\right] \tag{3.13}$$

can be computed. The z-coordinate, mass and the velocity of the i^{th} particle, and the force and the distance between particles i and j are denoted by z_i, m_i, v_i, F_{ij}, and r_{ij}, respectively. ΔV is the volume of one slice. The first sum in Eq. 3.13 is taken over all particles in a slice at position z and is proportional to their total kinetic energy. The second term, the virial term, takes the pressure contribution of the particle pair interactions into account. The function $f(z, z_i, z_j)$ assigns a weight to the virial depending on the position of the two particles i and j relative to a certain lateral slice:

$$f(z, z_i, z_j) = \begin{cases} \Theta(z_i - z)\Theta(z + \Delta z - z_i) \;\ldots\; z_i = z_j \\ \dfrac{1}{z_j - z_i}\displaystyle\int_{z_i}^{z_j} d\zeta\, \Theta(\zeta - z)\Theta(z + \Delta z - \zeta) \;\ldots\; otherwise \end{cases} . \tag{3.14}$$

Here $\Theta(z)$ is the Heavyside step function and Δz denotes the height of a slice. Eq. 3.14 can be interpreted as follows: If both particles are in the same slice, f equals 1. If neither of the particles is in the slice and the slice is between them, then $f = \Delta z/|z_j - z_i|$. If only one of the particles is in the slice, f is $dz/|z_j - z_i|$, with dz being the distance between the particle in the slice and the edge of the slice that points towards the particle outside the slice. In all other cases f = 0.

In literature pressure profiles generally describe the difference between the lateral pressure p_{LAT} and the pressure pointing towards the bilayer normal p_{ZZ}:

$$p(z)=\frac{p_{XX}(z)+p_{YY}(z)}{2}-p_{ZZ}(z)=p_{LAT}(z)-p_{ZZ}(z) \quad . \tag{3.15}$$

Since the influence of the lateral pressure on membrane proteins is equally important, our figures will also show the single pressure components, namely the lateral and the z-component. To ease comparison between the different concentrations, all pressure profiles were symmetrized.

Due to the fact that the surface tension γ of our simulated system is expected to be zero, its calculation allows to verify the computed pressure profiles. It is given by

$$\gamma=\int_{-h}^{h}(p_{ZZ}(z)-p_{LAT}(z))\,dz \quad , \tag{3.16}$$

where 2h denotes the height of the simulation box. In order to estimate the error of the pressure profiles, leading to a surface tension γ_0 not equal zero, we introduce the so-called “integral-equivalent constant” p_{IE} which can be derived from

$$\gamma=\gamma_0\neq 0\rightarrow\gamma_0=\int_{-h}^{h}p_{IE}\,dz=2\,h\,p_{IE}\rightarrow p_{IE}=\frac{\gamma_0}{2h} \quad . \tag{3.17}$$

In this way p_{IE} gives the constant pressure which p_{ZZ}-p_{LAT} would have to be shifted to obtain zero surface tension:

$$\int_{-h}^{h}p_{ZZ}(z)-p_{LAT}(z)-p_{IE}\,dz=0 \quad . \tag{3.18}$$

The resolution of the pressure profile is proportional to the finite number of lateral slices used for determining it. Due to this unavoidable lack of accuracy, the calculated surface tension will generally never be exactly zero. Nevertheless it allows to distinguish between a shift of the pressure and a non-sufficiency of accuracy: If an increase of the number of slices leads to a smaller absolute value of the surface tension, the mismatch results from the inaccuracy. If not, a constant shift of the pressure biases the results.

3.8 Moments of the lateral pressure

The n^{th} moment of the lateral pressure is given by

$$P_n = \int_0^{h_b} z^n \, p_{LAT}(z)\, dz \quad , \tag{3.19}$$

where h_b denotes the height of the monolayer. As shown in previous theoretical investigations [20], these moments are of high interest when trying to get information about the conformational equilibria of proteins that reside in the bilayer.

If the transition of a membrane protein from one state to another causes a change of its volume by ΔV, it has to work against the lateral pressure acting on it:

$$\begin{aligned} W &= -\int_{\Delta V} p_{LAT}(z)\, dV \\ &= -\int_{-h_b}^{h_b} p_{LAT}(z)\,(A_2(z) - A_1(z))\, dz = -\int_{-h_b}^{h_b} p_{LAT}(z)\,\Delta A(z)\, dz \end{aligned} \quad . \tag{3.20}$$

$A_1(z)$ and $A_2(z)$ denote the depth-dependent cross-sectional area of the protein before and after the transition. By expanding the cross-sectional areas into power series

$$A_n(z) = \sum_{j=0}^{\infty} a_{j,n} z^j \quad , \tag{3.21}$$

the difference between the cross-sections is given by

$$\Delta A(z) = A_2(z) - A_1(z) = \sum_{j=0}^{\infty} (a_{j,2} - a_{j,1}) z^j = \sum_{j=0}^{\infty} \Delta a_j z^j \tag{3.22}$$

and the work W can be expressed in terms of the lateral moments:

$$\begin{aligned} W &= -\sum_{j=0}^{\infty} \int_{-h_b}^{h_b} p_{LAT}(z)\, \Delta a_j z^j\, dz \\ &= -\sum_{j=0}^{\infty} \Delta \tilde{a}_j P_j \end{aligned} \quad . \tag{3.23}$$

Since the anesthetic is assumed to cause a change of the lateral pressure and thus to modify the moments, the work changes by

$$\Delta W = -\sum_{j=0}^{\infty} \int_{-h_b}^{h_b} \Delta p_{LAT}(z) \Delta a_j z^j dz = -\sum_{j=0}^{\infty} \Delta \tilde{a}_j \Delta P_j \quad , \tag{3.24}$$

which leads to a shift of the conformational equilibrium K of a protein:

$$K = K_0 e^{-\Delta W / k_b T} \quad . \tag{3.25}$$

K_0 denotes the conformational equilibrium constant of the protein in a membrane without anesthetic and T is the temperature of the system. A conformational shift is significant if $|-\Delta W/k_bT|$ is larger than ln(2), meaning that the equilibria at least differ by a factor of 2.

3.9 Geometric protein model

We use a simple protein model of bent helices as suggested by Cantor to estimate the conformational shift that can occur through the presence of an anesthetic [20]. In this case the cross-sectional area is determined by

$$A_n(z) = \pi \left[r_0 + |z| \tan \phi_n \right]^2 = \pi \left[r_0^2 + 2 r_0 |z| \tan \phi_n + z^2 \tan^2 \phi_n \right] \quad , \tag{3.26}$$

where r_0 is the constant radius of the circular cross-sectional area of the protein in the center of the bilayer and ϕ_n is the angle of inclination between the kinked helices and the bilayer normal. Due to the simplicity of this geometric model, in which the protein has a shape like an hourglass, only the first and second moments of the lateral pressure are of interest for the calculations and the difference between the cross-sectional areas of the initial (1) and the final (2) state is given by

$$A_2(z) - A_1(z) = \pi \left[2 r_0 |z| (\tan \phi_2 - \tan \phi_1) + z^2 (\tan^2 \phi_2 - \tan^2 \phi_1) \right] \quad . \tag{3.27}$$

Thereby, using Eq. 3.20, the total change of the work per monolayer is

$$\Delta W_{ML} = -\pi \left[2 r_0 (\tan \phi_2 - \tan \phi_1) \Delta P_1 + (\tan^2 \phi_2 - \tan^2 \phi_1) \Delta P_2 \right] \quad , \tag{3.28}$$

with ϕ_1 and ϕ_2 being the angles for the initial and the final state. These angles may differ for the monolayers due to the membrane protein's possible asymmetry. If the geometry of the protein is symmetric around the bilayer center, then $\Delta W = 2\ \Delta W_{ML}$. As one can see from the derivation, the anesthetic concentration-dependent variation of the work for opening the

model ion channel is directly proportional to the change of the first and second moment of the lateral pressure.

3.10 Membrane elastic properties

The moments can be used for the determination of different elastic properties of the bilayer. Especially the determination of the bending modulus κ is of high interest because it is a measure for the stiffness of the membrane. The product of the bending modulus and the spontaneous curvature c_0 is given by

$$\kappa c_0 = \int_0^{h_b} (z - z_s)\, p_{LAT}(z)\, dz = P_1 - z_s P_0 \tag{3.29}$$

and the Gaussian curvature elastic modulus κ_G can be calculated using

$$\kappa_G = P_2 - 2 z_s P_1 \quad . \tag{3.30}$$

In Eq. 3.29 and 3.30 z_s denotes the vertical position of the neutral surface at which small curvature deformations occur at constant molecular area [21].

4 Simulation details

All simulations were performed using the Gromacs 4.0 MD package [1]. The lipid bilayers used in this work consist of 200 POPC molecules, 5000 water molecules and, dependent on the concentration, of 0 to 16 ketamine molecules. As already mentioned, Berger lipids were used to describe the POPC and the OPLS-AA force field was used for ketamine (Sect. 2.1).

For the construction of the membrane (Fig. 4.1) the POPC molecules were at first put into an empty simulation box to form a bilayer with 100 molecules in each monolayer. This initial structure was then solvated with explicit SPC water [4], adding 25 water molecules per lipid (fully hydrated). Afterwards the ketamine molecules were randomly placed inside the bilayer and randomly rotated.

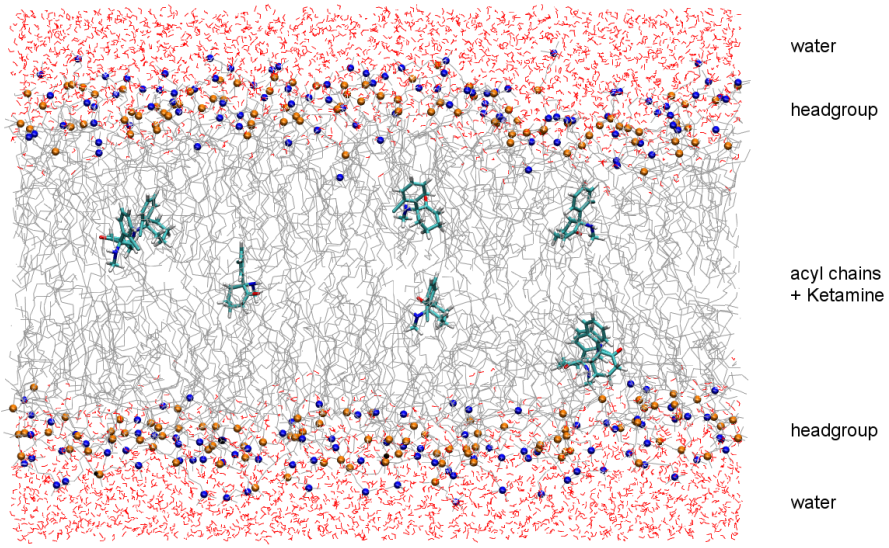

Fig. 4.1: Computational structure of hydrated membrane

The random placement of the molecules can cause two atoms to come too close to each other (overlap) and thus the resulting initial forces would be by far to high. To avoid this we first inflated the box and thereby the distance between the molecules by a factor of 5. Afterwards we performed several short energy minimization runs at a temperature of 10 K where we deflated the bilayer by a factor of 0.98 after each run until the area per lipid was 0.6 nm^2. The systems obtained in this way were then used to start the simulations covering a time frame of 100 ns, using an integration time step of 2 fs. Even though all simulated systems were already equilibrated after 20 ns, we only used the time frame between 50 and 100 ns for all analyses because we increased the output frequency of the simulation after 50 ns.

All the MD simulations were carried out using periodic boundary conditions. The neighbor search was conducted according to the grid method, updating the neighbor list every 10 steps and using a neighbor list cutoff of 1 nm. A constant temperature of 310 K (36.85 C) was maintained using the velocity rescale (v-rescale) algorithm (Sect. 2.2.6) with a τ_T of 0.1 ps. A pressure of 1 bar was established by performing semi-isotropic Berendsen pressure coupling with τ_P = 4.0 ps and a compressibility of 4.5 10^{-5} bar^{-1} (Sect. 2.2.7). Bond lengths were constrained using the Lincs method [12]. Coulomb energies were calculated according to PME electrostatics [16] with a cutoff of 1.0 nm and a PME order of 4. Van der Waal's energies were collected using a cutoff of 1.0 nm.

5 Results

5.1 Area per lipid

The area per lipid only slightly increases with higher ketamine concentration, as Fig. 5.1 shows. In our case the change between the highest and the lowest concentration is about 0.015 nm², with a maximum of approximately 0.69 nm² (see Tab. 5.1). The average standard deviation is ~0.0068 nm².

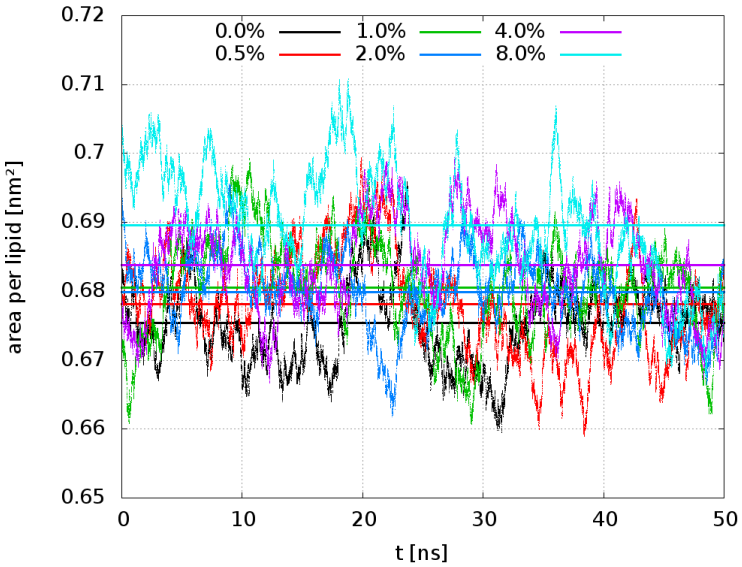

Fig. 5.1: Area per lipid

Concentration [%]	Area per lipid [nm²]	Standard deviation [nm²]
0.0	0.6754	0.00591
0.5	0.6781	0.00720
1.0	0.6805	0.00717
2.0	0.6799	0.00535
4.0	0.6838	0.00682
8.0	0.6900	0.00852

Tab. 5.1: Area per lipid

The increase of the area per lipid with higher concentrations arises from the local change of density that comes with the presence of the ketamine. Due to the mutual repulsion, the ketamine molecules do not come arbitrarily close to the acyl chains, meaning that they need additional space. This on the

other hand leads to a lateral enlargement of the simulation box and thereby to an increase of the area per lipid.

5.2 Position distributions

The vertical position distributions of the ketamines clearly show that they accumulate in a certain height above and below the center of the bilayer (Fig. 5.2). As one can see in Fig. 5.3, this height of approximately 1 nm is almost independent of the concentration of the anesthetic. This furthermore indicates that, at least for the concentrations we investigated, no mutual influence between the ketamine molecules could be recognized.

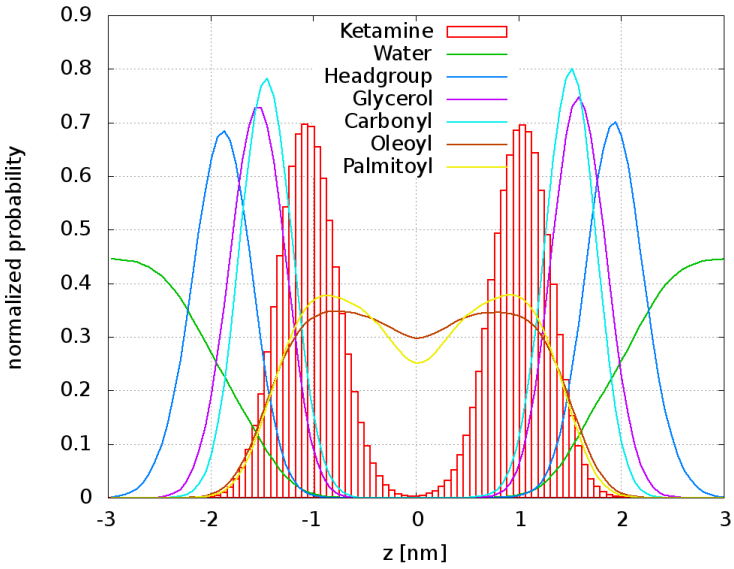

Fig. 5.2: Vertical position of various molecular groups

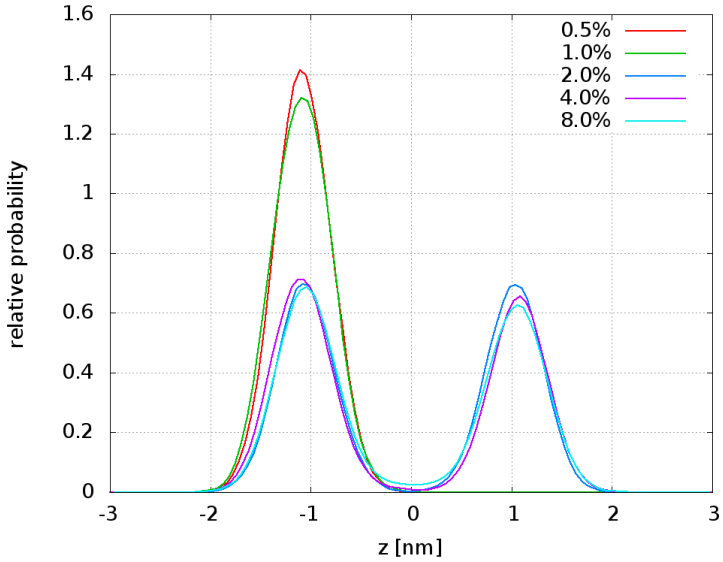

Fig. 5.3: Concentration-independence of vertical ketamine position

A comparison between the position distributions of the carbon atoms of the acyl chains and the one of the ketamine allows us to conclude that the anesthetic most likely resides close to the position of the 5th carbon-atom of the palmitoyl chain and the 6th carbon-atom of the oleoyl chain, respectively (Fig. 5.4).

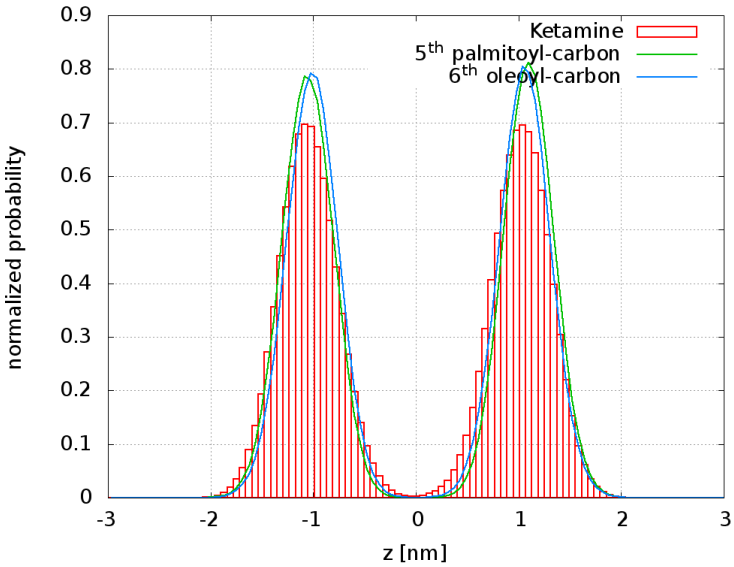

Fig. 5.4: Vertical position of nearest acyl chain carbons

The ketamine stays at a certain vertical position because the membrane provides a local energy minimum. Nevertheless, it can diffuse to the opposite side of the membrane (Fig. 5.5).

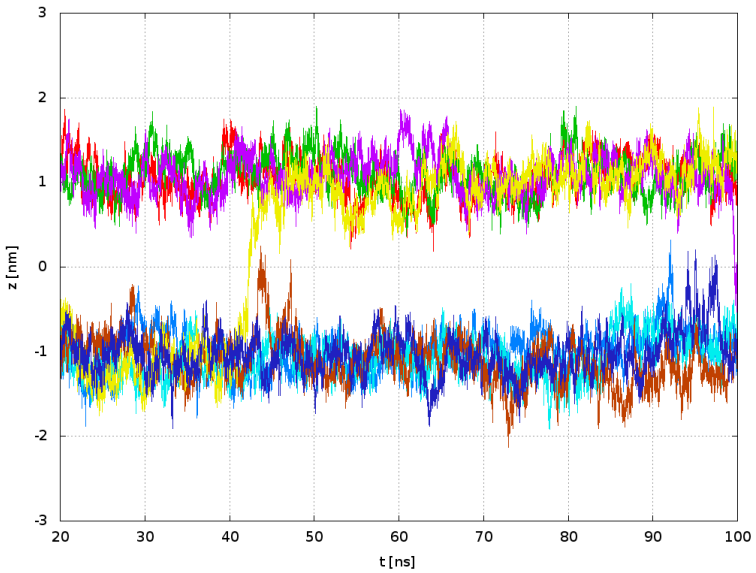

Fig. 5.5: Vertical movement of different ketamine molecules

The position distributions of the different characteristic atoms of the ketamine (Fig. 5.6) allow to highlight its orientation inside the bilayer. In our case the characteristic ketamine atoms are the oxygen (O), the nitrogen from the methylamino group (N), the chlorine (Cl) and the two carbons that connect the cyclohexane (C_{HEX}) and the chlorophenyl ring (C_{CPH}). The oxygen is closest to the headgroup which is not surprising because we would not expect the polar part to point towards the more lipophilic center. Since the nitrogen is like the oxygen connected to the cyclohexane, its orientational behavior is comparable to the one of the oxygen. A look at the trajectory reveals that the chlorine, attached to the phenyl ring, does not show the same behavior. Since the cyclohexane and the phenyl can be rotated against each other around the vector connecting them, the chlorine does sometimes point towards the outside and sometimes towards the inside of the membrane. For that reason the chlorine's position distribution is broader than the one of the oxygen.

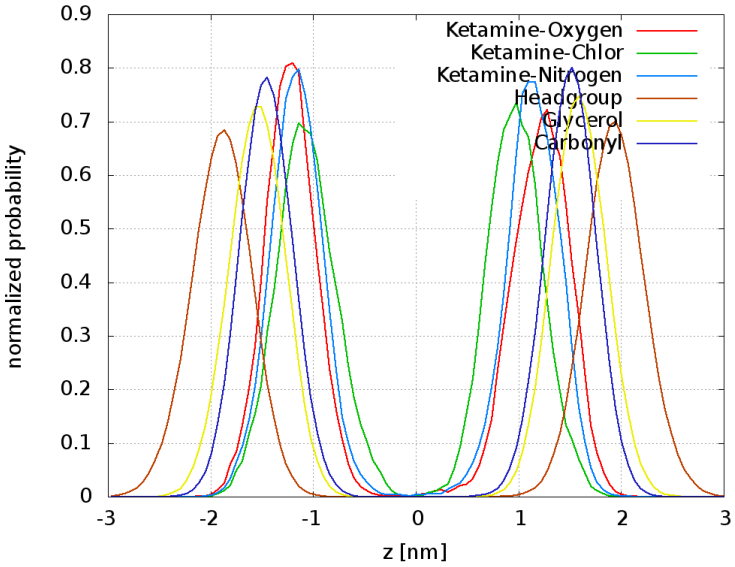

Fig. 5.6: Position of characteristic ketamine atoms

As expected, there is no preferred lateral position of the anesthetics in the membrane (Fig. 5.7). Starting from the initial coordinates, each molecule performs a random walk in the membrane plane. The distance, the molecules cover after a certain finite time, strongly varies from molecule to molecule which complicates the prediction of their diffusional behavior. Our trajectories are still on the short site for the analysis of the diffusion.

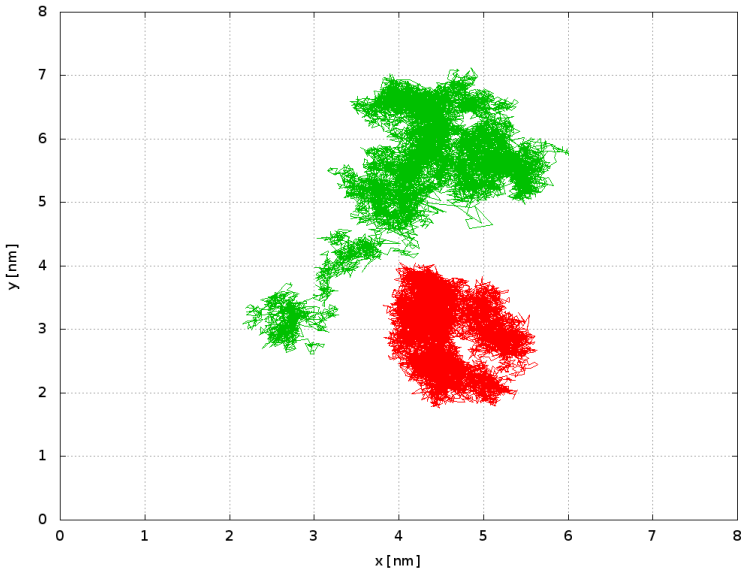

Fig. 5.7: Lateral movement of two selected ketamine molecules

5.3 Angle distributions

Figures 5.8, 5.9 and 5.10 show the normalized angle distributions for the POPC-headgroups and of both acyl chains. For the headgroup the vector between the phosphorus of the phosphate- and the nitrogen of the choline-group was taken into account. The distribution has a maximum at approximately 79 and at 101 degrees relative to the membrane normal, respectively, depending on whether the top or the bottom layer of the membrane is concerned. This means that the headgroups point only slightly towards the outside of the bilayer. For the acyl chains the vector between the first carbon after the carboxyl group and the terminal methyl group of the chain was used for the angle analysis. The distribution of the oleoyl has a maximum at about 29 and at 151 degrees, while for the palmitoyl chain the highest probability can be found at approximately 25 and 155 degrees. All these angle distributions are almost the same for all concentrations which means that the anesthetic does not seem to have a noticeable effect on them.

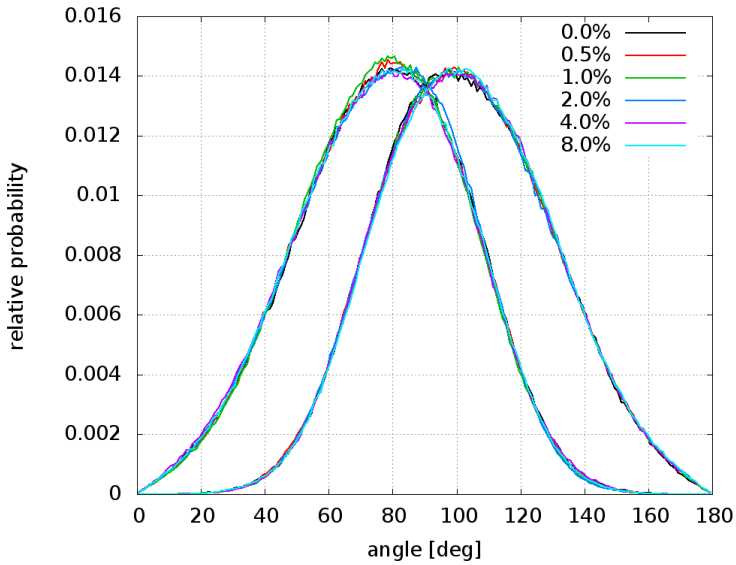

Fig. 5.8: Headgroup angle distribution

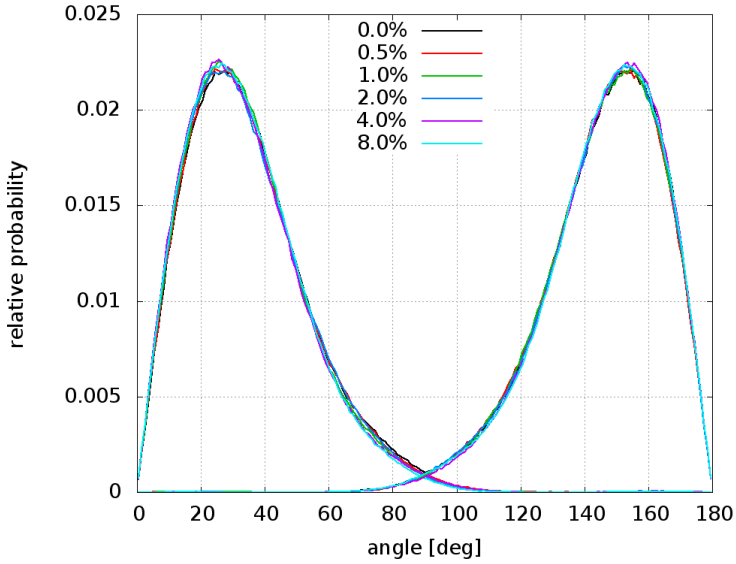

Fig. 5.9: Palmitoyl angle distribution

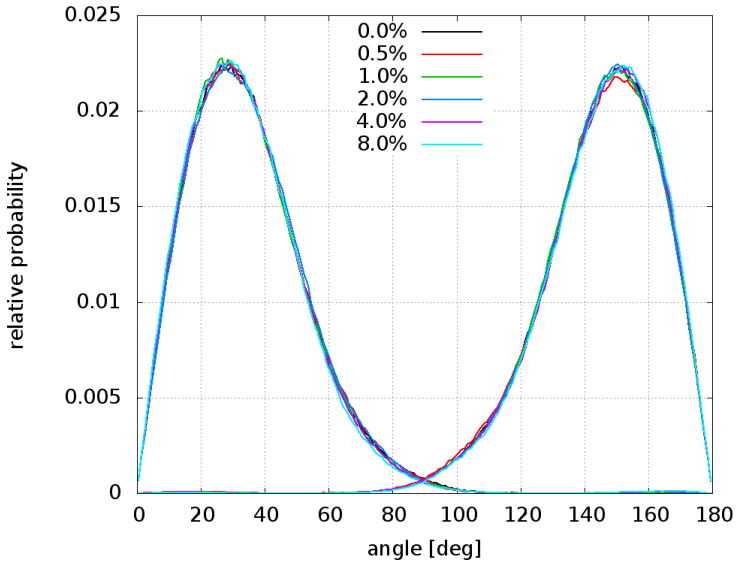

Fig. 5.10: Oleoyl angle distribution

The angle distributions for the ketamine's chlorine-oxygen- and the C_{CPH}-C_{HEX}-vector allow us to confirm the interpretation of the orientation obtained from the position distributions. As one can see in Fig. 5.11, these angle distributions are not as smooth as the ones of the POPC because much less ketamine molecules could be used for the statistical average. Since the ketamine molecule is small compared for example to the phospholipid, small relative changes in position between the cyclohexane and the phenyl ring lead to large changes of the angle between the chlorine and the oxygen and between C_{CPH} and C_{HEX}. For that reasons these angle distributions are broader than the ones obtained for the phospholipid headgroups and acyl chains. The asymmetry of the distributions between the two monolayers

arises from the small number of molecules available for determining the statistical average.

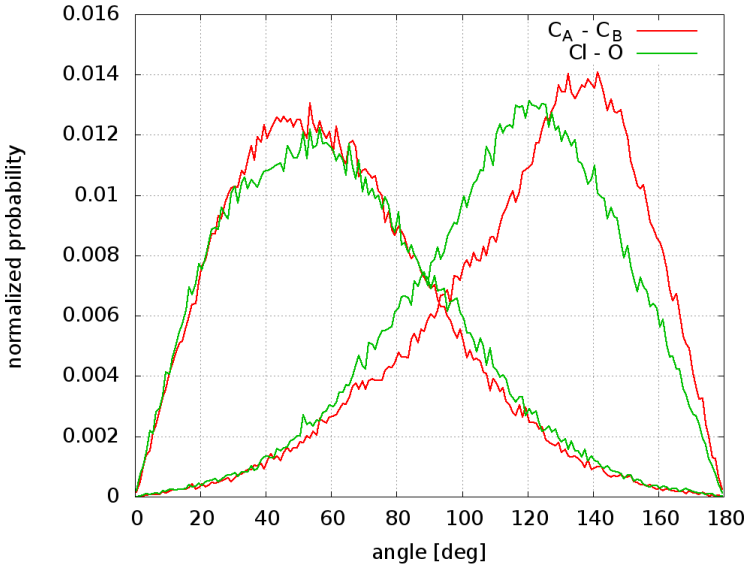

Fig. 5.11: Angle distributions for special ketamine groups

5.4 Order parameter

The obtained deuterium order parameters of the palmitoyl and the oleoyl chain are in good agreement with the data obtained from experiments [22]. Their comparisons for the different ketamine concentrations (Fig. 5.12 and 5.13) show an increase of the order parameter with higher concentrations. It is interesting to note that the largest difference between the order parameters for both acyl chains can be found between the 5^{th} and the 7^{th} carbon atom. As already mentioned before, this is approximately the position where the ketamine molecules most likely reside. For the carbon atoms which are closer to the center or closer to the headgroup the difference is much smaller.

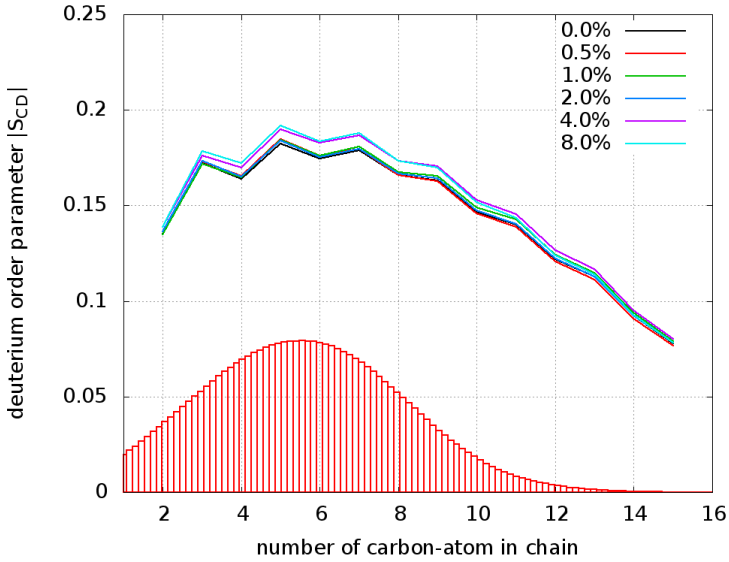

Fig. 5.12: Order parameter for palmitoyl chain

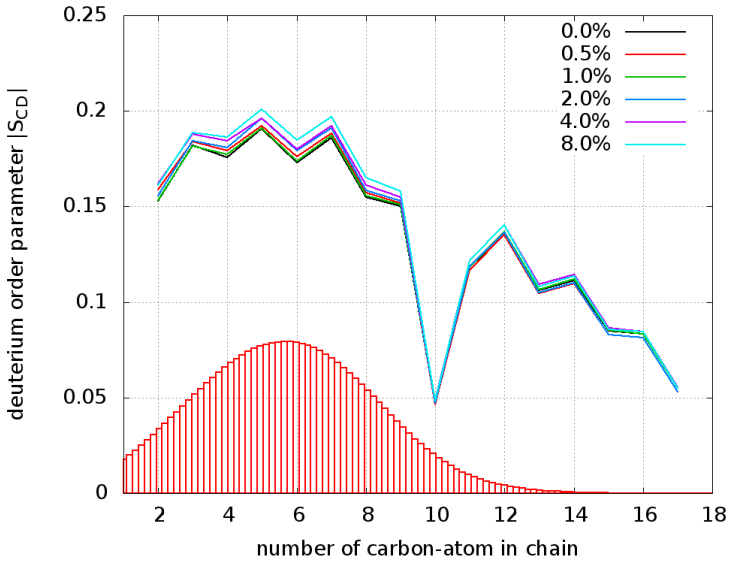

Fig. 5.13: Order parameter for oleoyl chain

These results combined with the information from the angle distributions allow to conclude that the anesthetics only seem to locally influence the order of the chain while the direction of the vector between the begin and the end of the fatty acid approximately stays the same. This means that only the local curvature of the chain is altered.

5.5 X-ray form factor

The computed form factors are in quite good agreement with the experimental data (Fig. 5.14). One has to turn attention to the fact that the

form factors only slightly change for the different concentrations. For all concentrations simulated, the deviation of the form factors from the one of the unanesthetized membrane is smaller than the error made in the experiment. Thus, x-ray scattering experiments, which are often used for the investigation of membrane structures, do probably not deliver the accuracy needed to recognize the influence of an anesthetic.

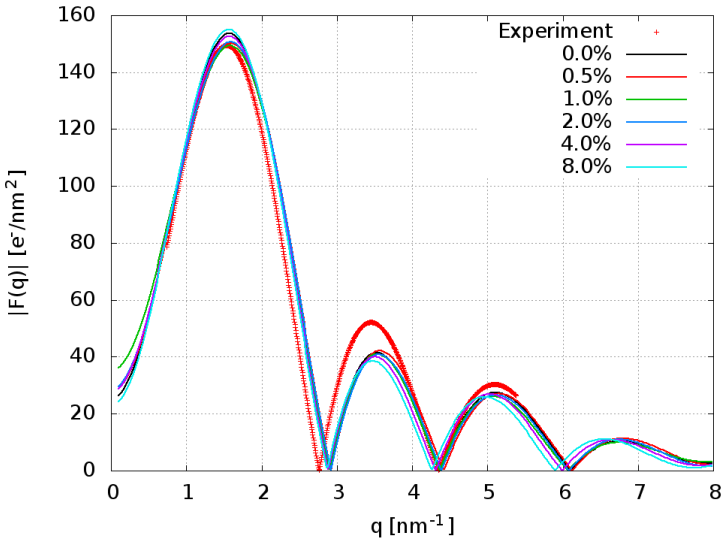

Fig. 5.14: Form factors for different concentrations compared with experimental values

5.6 Mean square displacement and diffusion coefficient

The mean square displacements shown in Fig. 5.15 confirm the expectation that the prediction of the anesthetics' diffusional behavior is difficult. The diffusion coefficients of the single ketamine molecules (Tab. 5.2) range from ~0.001 to ~0.376 [10^{-5}cm^2/s] which is a variation of more than 2 orders of magnitude. Thus the results do not allow to make concrete predictions about the diffusion of the anesthetic inside the membrane.

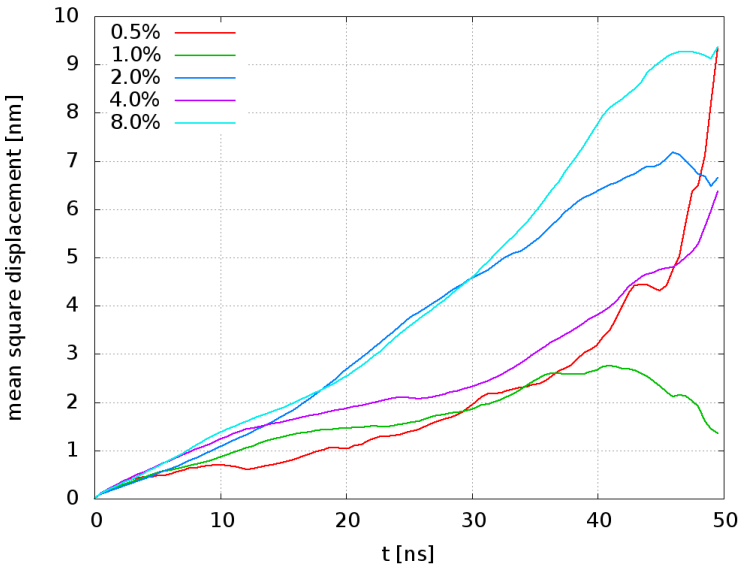

Fig. 5.15: Mean square displacements

Concentration [%]	Diffusion coefficient [10^{-5}cm²/s]			
0.5	0.0185173			
1.0	0.00800039	0.0205563		
2.0	0.0307594	0.0333883	0.0396296	0.0574406
4.0	0.00272544	0.023147	0.0238512	0.0195775
	0.0369357	0.0208973	0.0	0.0402795
8.0	0.00398408	0.10252	0.0971801	0.00513357
	0.00638738	0.0087023	0.0221889	0.0267876
	0.00139461	0.0102742	0.0155864	0.0124069
	0.0039912	0.00204373	0.0170728	0.376408

Tab. 5.2: Diffusion coefficients

It is surprising that the mean square displacement varies so much for the different ketamine concentrations and between the single molecules since in general the diffusion coefficients derived from them should approximately have the same value. In our case there are two reasons why such a non-conclusive result has been obtained: On the one hand we can only use a few ketamine molecules for the averaging of the mean square displacement. Furthermore the number of these molecules is concentration-dependent which leads to the fact that the average gets worse with decreasing concentration. On the other hand the simulation data used for the analyses only covers a time frame of less than 100 ns. Using Eq. 3.12 for determining the diffusion coefficient, one would need an infinite time frame to make exact predictions. So the smaller the investigated time frame, the bigger the uncertainties of the results. This is not unexpected, as diffusion in a membrane is very slow because a bilayer is a medium with high viscosity.

Two lipids for example exchange their place on a time scale of tens of nanoseconds.

5.7 Pressure profile

As shown in Fig. 5.16, the lateral pressure decreases with increasing ketamine concentration especially in regions where the anesthetic is most likely to be found. Elsewhere, like in the bilayer center, the pressure deviation is only very small. The difference between the pressures at the several concentrations and the pressure obtained from the simulation without ketamine clearly shows the significant change (Fig. 5.17). In some areas the deviation exceeds 120 bar for the highest concentration which is more than 15% of the total difference between the minimum and the maximum pressure. Furthermore the difference function has a maximum exactly at the most probable vertical ketamine position.

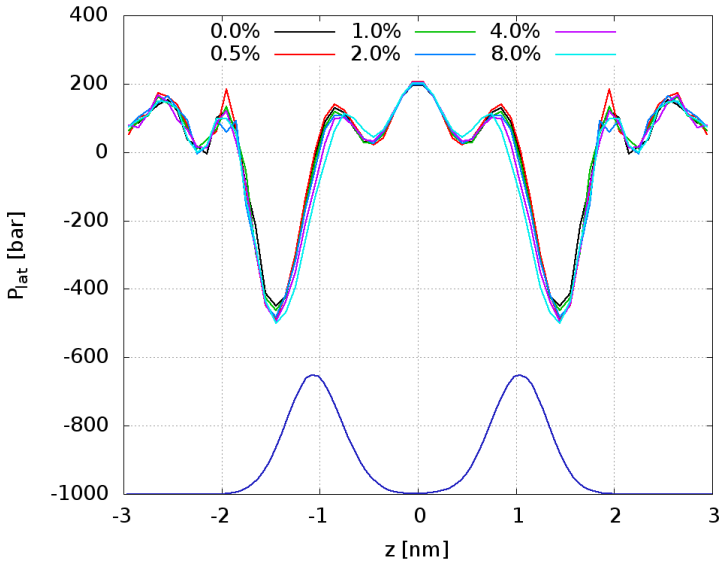

Fig. 5.16: Lateral pressure

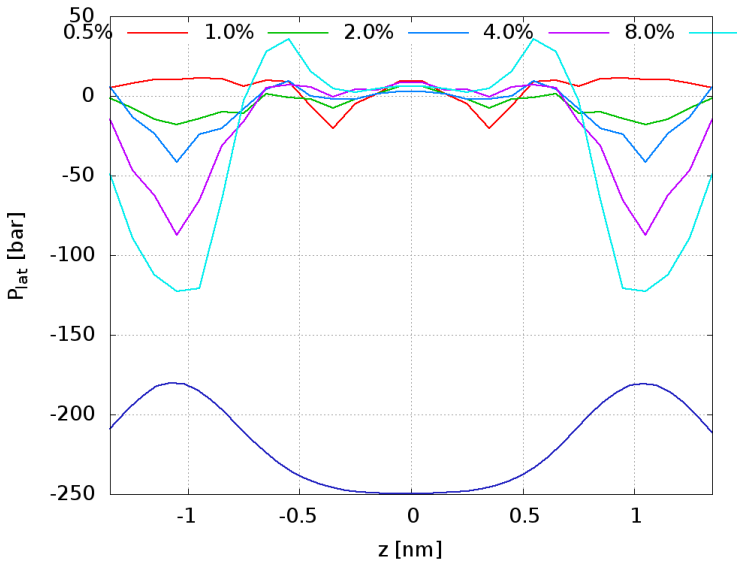

Fig. 5.17: Difference of lateral pressure compared to simulation without ketamine

The pressure component along the bilayer normal (Fig. 5.18) exhibits approximately the same qualitative behavior as the one from the lateral case, except that the maximum of the pressure deviation function has slightly moved towards the bilayer center (Fig. 5.19). The absolute value of the deviation is smaller, but the length at which a significant difference can be found has broadened.

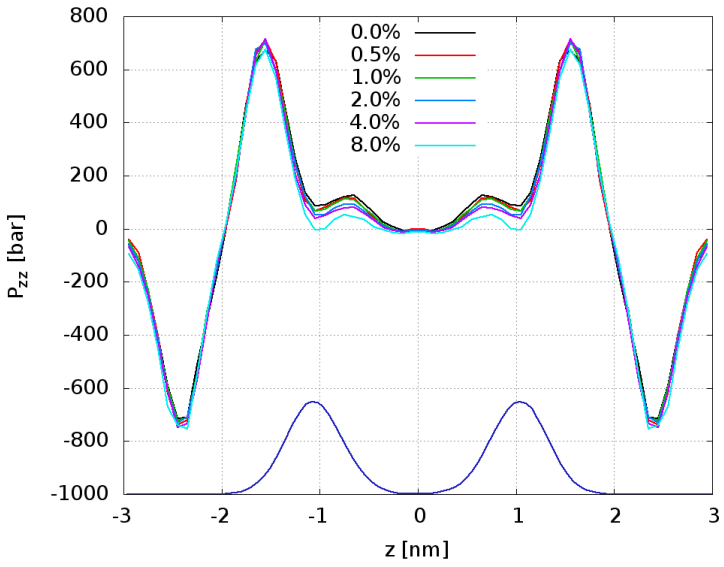

Fig. 5.18: Vertical pressure

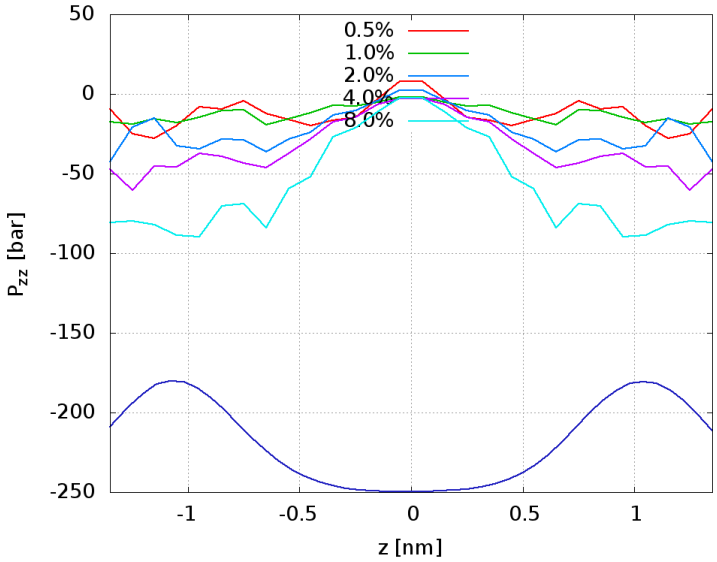

Fig. 5.19: Difference of vertical pressure compared to simulation without ketamine

The pressure profiles in Fig. 5.20 displaying p_{LAT}-p_{ZZ} do not differ as much from each other as the single components because the subtraction compensates most of the pressure decrease observed before. The small variation in p_{LAT}-p_{ZZ} leads to the result that the surface tension, which is almost zero for the bilayer without any ketamine, remains almost zero also for the other concentrations. The integral-equivalent constant (Sect. 3.7) slightly increases with higher concentrations, but on average the absolute value is only around 8 bar which is smaller than the error made in the simulations.

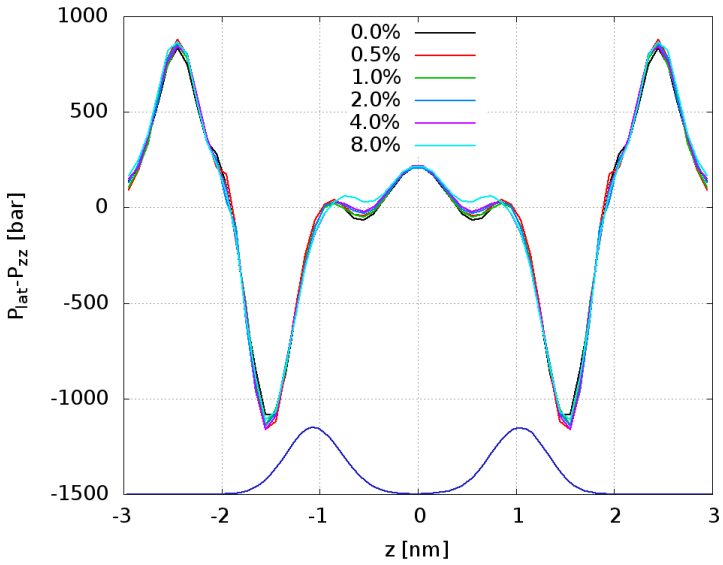

Fig. 5.20: Difference between lateral and vertical pressure

5.8 Moments of the lateral pressure

Table 5.3 shows the concentration-dependent first and second moments of the lateral pressure. The moments significantly increase towards higher concentrations. The relative changes of the moments range from ~8% for the lowest to more than 40% for the highest concentration. A comparison of P_1/k_bT and P_2/k_bT with the values derived theoretically and published by Cantor [20], namely $P_1/k_bT \sim -17\ nm^{-1}$ and $P_2/k_bT \sim -31.0$, shows that the simulations lead to higher values than predicted. The difference probably arises from the simplified model used for the theoretical deduction.

Concentration [%]	P_1/k_bT [nm^{-1}]	ΔP_1 [%]	P_2/k_bT [ ]	ΔP_2 [%]
0.0	-4.56		-6.72	
0.5	-4.90	7.48	-7.31	8.85
1.0	-5.11	11.94	-7.52	11.94
2.0	-5.74	25.90	-8.56	27.43
4.0	-6.09	33.66	-8.84	31.63
8.0	-6.62	45.23	-9.48	41.11

Tab. 5.3: First and second moments

Applying the protein model of bent helices discussed in Sect. 3.9, one can estimate the effect of the anesthetic on a protein's conformation. Figure 5.21 depicts $|\Delta W/k_bT| = \ln(2)$ for different concentrations, angles and angular changes. The radius r_0 of the model protein was set to 2 nm which is assumed to be representative for ligand-gated ion channels. Furthermore, an angular change of about 6° between the channel's opened and closed state can be expected [20]. The results show that even for the lowest concentration significant changes of the conformational equilibrium would occur already at angular changes $\Delta\phi = \phi_2 - \phi_1$ below 6° of an ion channel. Assuming that the predicted parameters for the ligand-gated ion channels are correct, the presence of the anesthetics indeed seems to influence the transmission behavior of these channels.

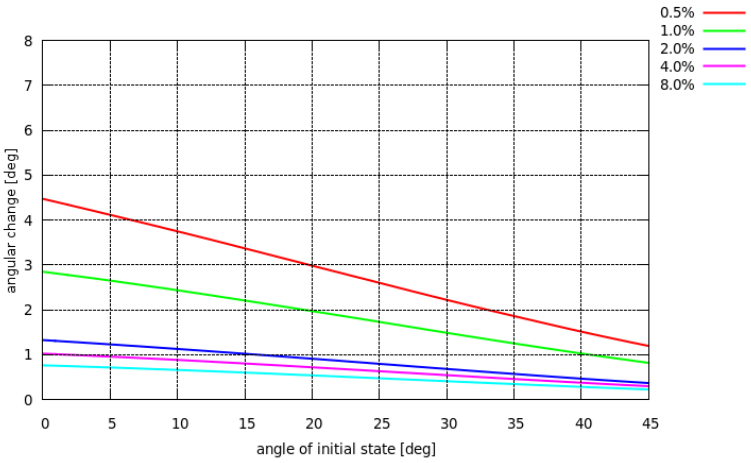

Fig. 5.21: Changes of protein conformation

Using Eq. 3.29 the bending modulus can be calculated from the first moment. Expecting a spontaneous curvature with radii in the nanometer scale, a bending modulus in the order of magnitude of ~10^{-20} J was found. This is in good agreement with the values obtained in earlier studies [23]. If we expect the spontaneous curvature to not change with varying anesthetic concentration, the increase of the absolute value of P_1 leads to an increase of the bending modulus, meaning that the bilayer becomes stiffer with higher concentrations.

In order to review our analyses we visualize the most important observables in Fig. 5.22. To give insight into a single simulation run we display the results for the highest ketamine concentration which exhibits the largest effects.

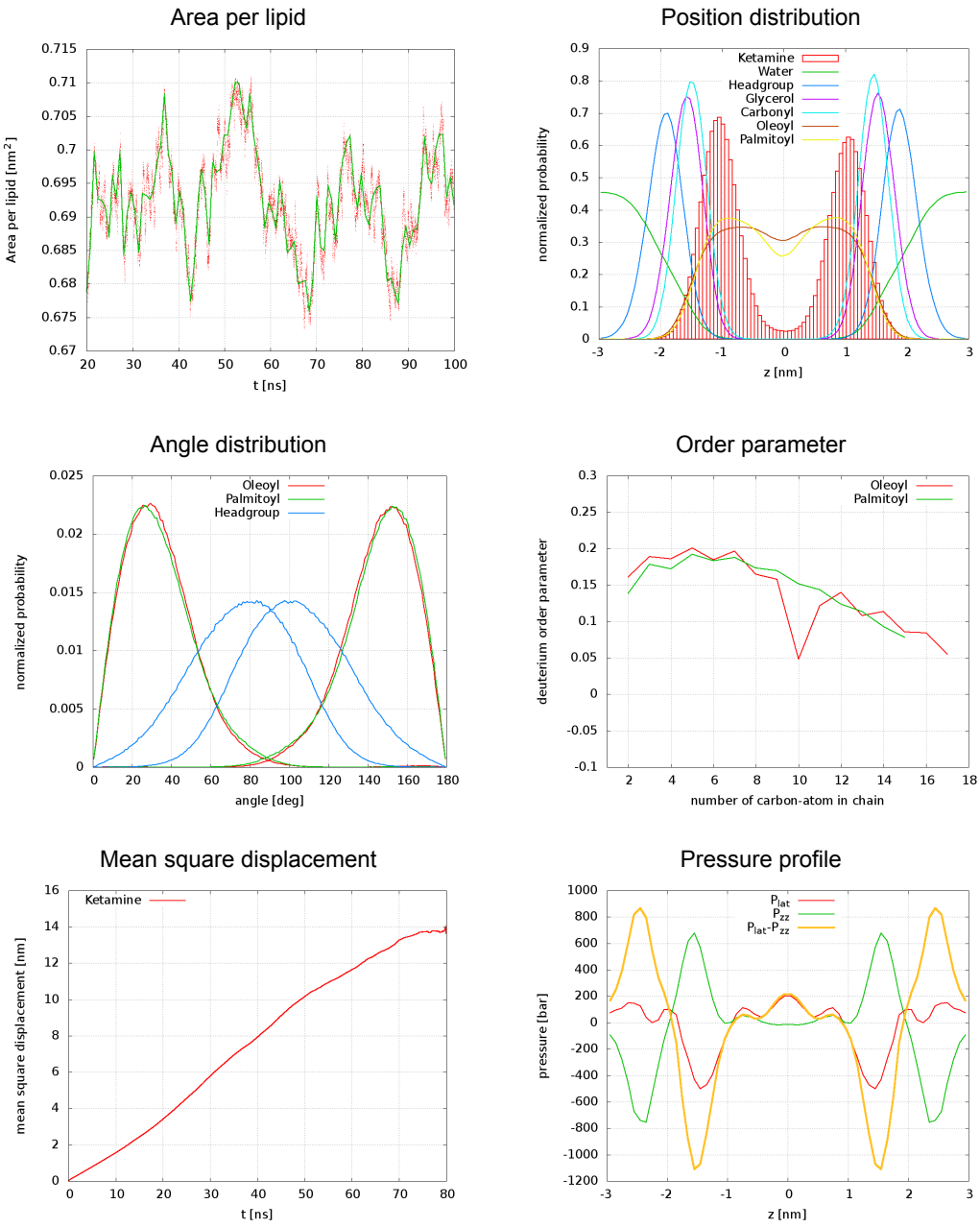

Fig. 5.22: Analyses of a single simulation run (8.0% ketamine)

6 Conclusions and Outlook

The obtained results clearly show that the ketamine molecules prefer to reside at certain vertical positions inside the membrane. Due to this preference the order parameters of the acyl chain carbon atoms feature the highest concentration-dependent deviations close to that positions. Furthermore, the lateral pressure declines with increasing concentration in this vertical regions. Thus we could relate the corresponding changes of the moments of the lateral pressure to changes of the conformational equilibrium of a model membrane protein. Thereby significant conformational shifts could be observed, even for the lowest concentration.

As the case of the x-ray form factor shows, some experimental methods that are commonly used today to determine various membrane parameters are probably not accurate enough to measure anesthetic-caused effects. Thus it will be necessary to improve these methods or invent new ones in order to further verify the results of the simulations.

In summary, all results leave no doubt that significant parameters of a phospholipid membrane definitely change through the presence of an anesthetic. They strongly support the theory of the mode of functioning of an anesthetic where it actually does not bind to membrane proteins or receptors, but influences the membrane in a simple mechanical way. This of course does not mean that the binding theory is wrong, but our results indeed allow to conclude that the pure mechanical effects, as suggested by Cantor [24], can not be neglected.

For future investigations, the main goal should be to find further indications that serve as a proof of the membrane theory. In our opinion research should be continued on:

- Enantiomer effect

  For the ketamine studied in this thesis, the enantiomer (chiral molecule) of the clinically active ketamine is known not to have the same anesthetic effect. Simulations using the enantiomer could further support the theory of the membrane pressure mediated anesthesia mechanism.

- Different kinds of anesthetics

  Due to the fact that we only considered one anesthetic molecule in all our simulations, it would be useful to investigate the effects of other anesthetics applied in medicine. This would allow to determine whether the effect that causes the anesthesia is always the same or not. Furthermore one can try to relate the effectiveness of

anesthetics to a relative change of certain membrane parameters.

Of course there is a wide range of cases worth to be studied, but performing research on representative ones like the enantiomer is probably the best and least time-consuming approach.

References

[1] D. van der Spoel, E. Lindahl, B. Hess, Gromacs 4.0 User Manual, 2006

[2] O. Berger, O. Edholm, F. Jahnig, Molecular Dynamics Simulations of a Fluid Bilayer of Dipalmitoylphosphatidylcholine at Full Hydration, Constant Pressure, and Constant Temperature, Biophys. J., Vol. 72, p. 2002, 1997

[3] W. L. Jorgensen, D. S. Maxwell, J. Tirado-Rives, Development and Testing of the OPLS All-Atom Force Field in Conformational Energetics and Properties of Organic Liquids, J. Am. Chem. Soc., Vol. 118, p. 11225, 1996

[4] H. J. C. Berendsen, J. P. M. Postma, W. F. van Gunsteren, J. Hermans, INTERACTION MODELS FOR WATER IN RELATION TO PROTEIN HYDRATION, Intermolecular Forces, p. 331, 1981

[5] Jirasak Wong-ekkabut, Zhitao Xu, Wannapong Triampo, I-Ming Tang, D. P. Tieleman, L. Monticelli, Effect of Lipid Peroxidation on the Properties of Lipid Bilayers: A Molecular Dynamics Study, Biophys. J., Vol. 93, p. 4225, 2007

[6] R. W. Hockney, S. P. Goel, J. Eastwood, Quiet highresolution computer models of a plasma, J. Comp. Phys., Vol. 14, p. 148, 1974

[7] L. Verlet, Computer experiments on classical fluids. i. thermodynamical properties of lennard-jones molecules, Phys. Rev., Vol. 159, p. 98, 1967

[8] J. C. Butcher, The Numerical Analysis of Ordinary Differential Equations: Runge-Kutta and General Linear Methods, Wiley-Interscience, 1987

[9] J. C. Butcher, Numerical Methods for Ordinary Differential Equations, John Wiley & Sons, 2003

[10] S. C. Harvey, R. K. Z. Tan, T. E. Cheatham, The flying ice cube: Velocity rescaling in molecular dynamics leads to violation of energy equipartition, J. Comp. Chem., Vol. 19 (7), p. 726, 1998

[11] J. P. Ryckaert, G. Ciccotti, H. J. C. Berendsen, Numerical integration of the cartesian equations of motion of a system with constraints; molecular dynamics of n-alkanes, J. Comp. Phys., Vol. 23, p. 327, 1977

[12] B. Hess, H. Bekker, H. J. C. Berendsen, J. G. E. M. Fraaije, LINCS: A linear constraint solver for molecular simulations, J. Comp. Chem., Vol. 18, p. 1463, 1997

[13] H. J. C. Berendsen, J. P. M. Postma, A. DiNola, J. R. Haak, Molecular dynamics with coupling to an external bath, J. Chem. Phys., Vol. 81, p. 3684, 1984

[14] G. Bussi, D. Donadio, M. Parrinello, Canonical sampling through velocity rescaling, J. Chem. Phys., Vol. 126, p. 014101, 2007

[15] R. H. Byrd, P. Lu, J. Nocedal, A limited memory algorithm for bound constrained optimization, SIAM J. Scientif. Statistic. Comput., Vol. 16, p. 1190, 1995

[16] T. Darden, D. York, L. Pedersen, Particle mesh Ewald: An N-log(N) method for Ewald sums in large systems, J. Chem. Phys., Vol. 98, p. 10089, 1993

[17] J-P. Douliez, A. Ferrarini, E.-J. Dufourc, On the relationship between C-C and C-D order parameters and its use for studying the conformation of lipid acyl chain in biomembranes, J. Chem. Phys, Vol. 109, p. 2513, 1998

[18] S. A. Pandit, See-Wing Chiu, E. Jakobsson, A. Grama, H. L. Scott, Cholesterol Surrogates: A Comparison of Cholesterol and 16:0 Ceramide in POPC Bilayers, Biophys. J., Vol. 92, p. 920, 2007

[19] J. H. Irving, J. G. Kirkwood, The statistical mechanical theory of transport processes, J. Chem. Phys., Vol. 18, p. 817, 1950

[20] R. S. Cantor, The influence of membrane lateral pressure on simple geometric models of protein conformational equilibria, Chem. Phys. Lipids, Vol. 101, p. 45, 1999

[21] S. Ollila, T. Róg, M. Karttunen, I. Vattulainen, Role of sterol type on lateral pressure profiles of lipid membranes affecting membrane protein functionality: Comparison between cholesterol, desmosterol, 7-dehydrocholesterol and ketosterol, J. Struct. Biol., Vol. 159, p. 312, 2007

[22] S. Ollila, M. T. Hyvönen, I. Vattulainen, Polyunsaturation in Lipid Membranes: Dynamic Properties and Lateral Pressure Profiles, J. Phys. Chem. B, Vol. 111, p. 3139, 2007

[23] E. Lindahl, O. Edholm, Mesoscopic Undulations and Thickness Fluctuations in Lipid Bilayers from Molecular Dynamics Simulations, Biophys. J., Vol. 79, p. 426, 2000

[24] R. S. Cantor, The Lateral Pressure Profile in Membranes: A Physical Mechanism of General Anesthesia, Biochemistry, Vol. 36, p. 2339, 1997